AERODYNAMIC INFLUENCE COEFFICIENT METHOD USING SINGULARITY SPLINES

by J. E. Mercer, J. A. Weber, and E. P. Lesferd

1. Report No.	2. Government Accession No.	3. Recipient's Catalog No.
NASA CR- 2423		

4. Title and Subtitle	5. Report Date
"Aerodynamic Influence Coefficient Method Using Singularity Splines"	MAY 1974
	6. Performing Organization Code

7. Author(s)	8. Performing Organization Report No.
J. E. Mercer, J. A. Weber, and E.P. Lesferd	D6-41093
	10. Work Unit No.

9. Performing Organization Name and Address	
The Boeing Company, Commercial Airplane Co. P.O. Box 3707 Seattle, Washington 98124	11. Contract or Grant No.
	NAS 2-6530
	13. Type of Report and Period Covered

12. Sponsoring Agency Name and Address	Final Report 7/1/71 - 10/31/72
National Aeronautics & Space Administration Washington, D.C. 20546	14. Sponsoring Agency Code

15. Supplementary Notes

16. Abstract

A new numerical lifting surface formulation, including computed results for planar wing cases is presented. This formulation, referred to as the "vortex spline" scheme, combines the adaptability to complex shapes offered by paneling schemes with the smoothness and accuracy of loading function methods. The formulation employes a continuous distribution of singularity strength over a set of panels on a paneled wing. The basic distributions are independent, and each satisfies all the continuity conditions required of the final solution. These distributions are overlapped both spanwise and chordwise (termed "spline"). Boundary conditions are satisfied in a least square error sense over the surface using a finite summing technique to approximate the integral. The current formulation uses the elementary horseshoe vortex as the basic singularity and is therefore restricted to linearized potential flow. As part of the study, a non planar development was considered (i.e., interference shell body representation), but the numerical evaluation of the lifting surface concept was restricted to planar configurations. Also, a second order sideslip analysis based on an asymopototic expansion was investigated using the singularity spline formulation.

17. Key Words (Suggested by Author(s))	18. Distribution Statement
Lifting Surface Theory Wings & Bodies Aerodynamic Influence Coefficients Second Order Solutions Spline Least Squares	UNCLASSIFIED – UNLIMITED CAT. 01

19. Security Classif. (of this report)	20. Security Classif. (of this page)	21. No. of Pages	22. Price*
UNCLASSIFIED	UNCLASSIFIED	100	$4.00

*For sale by the National Technical Information Service, Springfield, Virginia 22151

CONTENTS

FIGURES

iv

TABLES

v

AERODYNAMIC INFLUENCE COEFFICIENT METHOD

USING SINGULARITY SPLINES

By J. E. Mercer, J. A. Weber
and E. P. Lesferd
The Boeing Company

1.0 SUMMARY

A new numerical lifting surface formulation, including computed results for planar wing cases is presented. This formulation, referred to as the "vortex spline" scheme, combines the adaptability to complex shapes offered by paneling schemes with the smoothness and accuracy of loading function methods. The formulation employs a continuous distribuution of singularity strength over a set of panels on a paneled wing. The basic distributions are independent, and each satisfies all the continuity conditions required of the final solution. These distributions are overlapped both spanwise and chordwise (termed "spline"). Boundary conditions are satisfied in a least square error sense over the surface using a finite summing technique to approximate the integral. The current formulation uses the elementary horseshoe vortex as the basic singularity and is therefore restricted to linearized potential flow. As part of the study, a non planar development was considered (i.e., interference shell body representation), but the numerical evaluation of the lifting surface concept was restricted to planar configurations. Also, a second order sideslip analysis based on an asymptotic expansion was investigated using the singularity spline formulation.

2.0 INTRODUCTION

Various lifting surface schemes have been proposed for the analysis of arbitrary wing planforms. Most of these methods treat this fluid dynamic problem by relating one flow parameter to another (e.g., downwash to pressure jump). A majority of the approaches can be characterized as constructing a solution from a composite of basic, assumed distributions of pressure, vorticity, or potential, all of which satisfy the governing differential equation. The boundary conditions of the problem determine the relative magnitudes of the various distributions. Each of these assumed distributions can cover the entire lifting surface or merely portions of it, depending on the particular numerical scheme.

Although many of the schemes arise from the above described common origin, in practice there can be great differences among them. As an example, consider the constant pressure panel (Ref. 1) and pressure mode (Ref. 2) schemes. The constant pressure panel scheme uses a single type of distribution that is of constant pressure ranging over some small region of a wing. A solution using this method is one that consists of a set of steps in the pressure level which can only roughly approximate the true solution. However, the method is applicable to both subsonic and supersonic flows and ranges over a wide variety of planform shapes. The pressure mode scheme, on the other hand, uses several different types of distributions ranging over all or at least a large portion of a wing. The solution using this method can yield very accurate pressure results. However, the method requires careful attention to discontinuities in supersonic flow and it is restricted in the geometry of planforms which it can treat. In choosing between these two schemes, trades between pressure details and generality of configurations must be weighed.

The FLEXSTAB system (Ref. 3) which performs the stability and control analysis of elastic arbitrary wing-body configurations was developed using the constant pressure panel scheme because of the schemes planform generality. Using this aerodynamic method, the program generates not only symmetric stability derivatives (e.g., C_{L_α}, C_{M_α}, etc.), but also antisymmetric stability derivatives (e.g., C_{ℓ_β}, C_{N_β}, etc.). It was soon recognized, however, that configurations with small wing dihedral could not be accurately analyzed for certain of their antisymmetric derivatives, specifically the rolling moment derivative, C_{ℓ_β}. Upon examination, it was discovered that the accuracy of the constant pressure panel scheme was not adequate for the analysis of these configurations. In an attempt to establish the requirements necessary to treat such cases, a study was performed (Ref. 4). This study, based on an asymptotic expansion of the differential equation in terms of the governing flow variables (e.g., angle-of-

attack and angle of sideslip), revealed that gradients of the pressure distribution appear to play as active a role in the sideslip problem of configurations with small dihedral as the pressures themselves. This result confirmed the belief that the constant pressure panel scheme could not treat this problem. Further investigation of other lifting surface schemes which might be applicable was initiated. This study concluded that no existing scheme could provide the needed pressure gradient accuracy required for the small dihedral configurations and at the same time, provide the desired generality. Accordingly, research to create a new scheme was begun. The result of this study was the development of the "vortex spline" scheme: a method which satisfies the above mentioned requirements. The key features of this method are:

1) The use of independent, overlapping singularity distributions which are arranged such that the final solution for the pressure will automatically be continuous in both value and slope (unless specifically required not to be at certain locations)

2) The use of wing paneling to provide a basis for the extent of coverage for each distribution, thereby giving it the generality of the constant pressure panel method

3) The satisfaction of boundary conditions using a least square error technique

4) The application to both subsonic and supersonic flow

5) The use of "special Mach lines" for paneling in supersonic flow.

The current formulation of the scheme is restricted to linearized, steady, potential flow. The restriction to linearized flow is due mainly to the use of the elementary horseshoe vortex as the basic singularity strength. This singularity was selected because of its automatic treatment of the linearized wake boundary condition and its compatability with the existing FLEXSTAB aerodynamic representation.

This report includes: 1) the derivation of the numerical scheme for flat wings of zero thickness along with computed results, 2) the description of a compatible interference shell representation (Ref. 1), 3) the description of a second order numerical scheme to compute interaction effects such as those which dominate for small dihedral, and 4) an alternate supersonic scheme studied initially (included in the appendix).

3

a   amplitude of quadratic addition to panel edge, also used as a coefficient of the equation for a panel edge.

A_C strength of Cauchy singularity

a_i area associated with ith control point

A_{ij} aerodynamic influence coefficient, an element of $\begin{bmatrix} A \end{bmatrix}$

A_L strength of logarithmic singularity

A_M strength of Mangler singularity

A_0 strength of non-singular terms evaluated at the singularity.

$\tilde{A}{}^T$ weighted transpose of influence coefficient matrix.

b   coefficient of the equation for a panel edge

$B_{II,I}$ influence coefficient representing the effect of Subdivision I on Subdivision II

c   coefficient of the equation for a panel edge

$\bar{c}$ average wing chord

$c(\eta)$ panel chord variation ($x_{TE} - x_{LE}$)

C_ℓ section lift coefficient

C_L wing lift coefficient

C_p pressure coefficient

E^2 square error

G_1 integral of the kernel function in the x direction (linear in x variation of vorticity)

G_2 integral of the kernel function in the x direction (constant in x variation in vorticity)

$\bar{G}$ numerical representation of G_1 and G_2

K   kernel function

M	Mach number, also, number of control points
N	number of spline functions
N_o	neutral point
P	pressure
r	cylindrical coordinate and also Mach line coordinate
R_j	roots of Mach line - panel edge equation (intersections of Mach line with panel edge)
s	area of integration and also Mach line coordinate
S_j	strength associated with function γ_j , an element of $\{s\}$
u	perturbation velocity in x direction divided by U_∞
U_∞	free stream velocity
v	perturbation velocity in y direction divided by U_∞
w	perturbation velocity in z direction divided by U_∞
w_i	downwash on control point, i
w_{ij}	downwash on control point i, due to spline function, j
W'	downwash on downstream subdivision due to upstream subdivision (used in supersonic flow)
W_{BC}	downwash specified by boundary conditions
W_S	downwash from spline functions
x	Cartesian coordinate
$\bar{x}$	nondimensional x coordinate
x^{ℓ}	segment of chordwise vorticity spline variation (ℓ is an index, not a power)
y	Cartesian coordinate
γ^n	segment of spanwise vorticity spline variation (n is an index, not a power)
$\dot{\gamma}^n$	$\partial \gamma^n / \partial y$ (n is an index, not a power)

$\bar{y}$	nondimensional y coordinate
z	Cartesian coordinate
α	angle of attack
β	$\sqrt{1-M^2}$ (subsonic) or $\sqrt{M^2-1}$ (supersonic)
$\epsilon_1, \epsilon_2, \epsilon_3$	small distance from singularity (used to evaluate $\bar{G}$)
γ	bound vorticity
γ_j	spline function vorticity distribution
δP	perturbation in pressure
ΔC_p	jump in pressure coefficient across wing surface
Δ slope	jump in panel edge slope
$\Delta x_1, \Delta x_2$	quadratic additions to panel edges
ζ	running coordinate in x direction
η	running coordinate in y direction
σ	shed vorticity
θ	cylindrical coordinate
$\bar{\theta}$	nondimensional θ coordinate
θ	circumferential vorticity spline variation
ρ	density of fluid
ϕ	perturbation velocity potential
ϕ_d	potential due to a point doublet
ϕ_s	potential due to a point source
ϕ_v	potential due to an elementary horseshoe vortex
$\Delta\phi$	jump in potential

Matrix Notation

$[A]$ matrix of elements, A_{ij}

$\lceil a \rceil$ diagonal matrix of elements, a_i

$\{ S \}$ vector of unknown strengths, S_j

$\{ W_{BC} \}$ vector of known boundary conditions

$[\ ]^T$ transpose of matrix

$\{\ \}$ vector

$[\ ]^{-1}$ inverse of matrix

Subscripts

H homogeneous solution to differential equation

i control point evaluation

ℓ lower surface

L left panel edge

LE leading edge

ML Mach line

o define location of singularity on shell surface

P particular solution to differential equation

R regular (non singular variable) and also right panel edge

S singular variable

TE trailing edge

u upper surface

4.0 REQUIREMENTS FOR NUMERICAL SCHEME

Before developing a new scheme, a set of requirements and desirable features was established. The requirements were based on 1) ultimately incorporating the scheme into FLEXSTAB and 2) the analysis performed in reference 4 (the latter because the main objective was to model flows around configuration with small geometric dihedral). The desirable features were based on experience with various lifting surface schemes.

The requirement set forth in reference 4 was that any numerical shceme that is to be used for interaction flow analysis (e.g., sideslip-angle of attack) must be capable of predicting gradients of pressure to the same degree of accuracy as most techniques currently predict pressure levels. This implies that the basic equivalent pressure distribution used to construct the solution must vary linearly as a minimum. A linear variation could approximate pressure gradients in the same way the constant pressure panel scheme approximates pressure levels.

A further requirement, established by the ultimate desire to incorporate the final result into FLEXSTAB, was that the new technique must be adaptable to arbitrary planforms. From experience with both pressure mode techniques and paneling techniques it was felt that treatment of arbitrary configurations can best be achieved through a paneling technique. Such techniques divide a configuration into many parts (called panels). A distribution of flow singularities is associated with each panel and therefore, these singularities conform to very complex geometries by mere adjustments to the panel sizes, shapes, and orientations.

Experience using various numerical schemes also showed that difficulties arise when attempting to model a lifting surface which is in the wake of another (e.g., a tail behind a wing). The source of the problem is singularities in the downwash field inherent in various numerical formulations. Because of these singularities, the downwash influence is only correct at discrete points in the flow field. For paneling techniques (which constitute the major source of this problem) this means that the trailing surface's paneling is determined by the leading surface's paneling or vice versa (which ever provides the more stringent requirement). When dealing with arbitrary configurations many such paneling problems can arise thus causing much time to be spent establishing the paneling arrangement and in many cases, causing more panels to be used than would be for methods that do not produce downwash singularities. This was not considered acceptable, therefore the requirement was established to eliminate as many of these singularities as practical.

8

As a desirable feature, it was felt that a basic scheme applicable to both subsonic and supersonic flow would be ideal. Although not a requirement, such an arrangement could reduce the coding needed to implement the scheme and at the same time allow a single mathematical model to be analyzed all the way from incompressible flow through the supersonic regime.

Finally, the most desirable general possible approach would be a single basic scheme which could be used for both analysis and design. This again would greatly reduce coding and at the same time permit the user to almost arbitrarily switch analysis and design functions while designing an aircraft. As an example, a designer could generate a shape for a given flight condition and then analyze this configuration "off design" all in one run - greatly speeding up the design process.

Summarizing then, the general requirements are:

1) Capability to model pressure gradients

2) Arbitrary planform modeling

3) Minimum downwash singularities in flow field

The general desirable features are:

1) Unified approach for both subsonic and supersonic flow

2) A single basic scheme for both design and analysis.

Before any development of a new scheme was begun, a study of the characteristics of both subsonic and supersonic flow was undertaken to establish some of the more detailed numerical considerations. For subsonic linearized flow the properties can be summarized as:

1) A singularity in the pressure or bound vorticity at the leading edge which varies as the reciprocal of the square root of the distance from the edge - this causes the flow to turn abruptly at the leading edge.

2) The Kutta condition at the trailing edge (vanishing bound vorticity or pressure) - this is required to make the analysis mathematically unique and physically arises from viscous effects.

For supersonic, linearized flow there are several features to be considered:

1) Hyperbolic nature - a solution can proceed from fore to aft on a configuration.

2) Limited regions of influence - disturbances are limited to the interior of Mach cones and tend to concentrate most strongly along Mach cone boundaries.

3) Differing edge conditions - depending on the sweep of an edge with respect to a Mach line, the character of the solution differs: supersonic leading edges exhibit regular behavior whereas subsonic ones show a singular behavior. Subsonic trailing edges require a Kutta condition, whereas supersonic ones do not.

4) Discontinuous nature of flow across "special Mach lines" (those emanating from planform edge breaks - Fig. 1) - along special Mach lines the surface pressure and vorticity distribution can exhibit discontinuous behavior in levels and for gradients. Within regions bounded by these special Mach lines the flow exhibits a smooth regular behavior.

Various schemes use different means to represent the above characteristics and in many cases the characteristics are only approximated; yet, these approximations yield adequate results. Therefore, it is not an absolute modeling requirement that a new numerical formulation possess the ability to exactly represent all of the above characteristics; it is only necessary to carefully study the impact of each in the evaluation of the scheme.

The next section contains the analysis used to develop a new numerical scheme, the vortex spline, along with the computed results. The appendix contains another method for supersonic flow only, the doublet characteristic box, which was investigated but not fully developed.

10
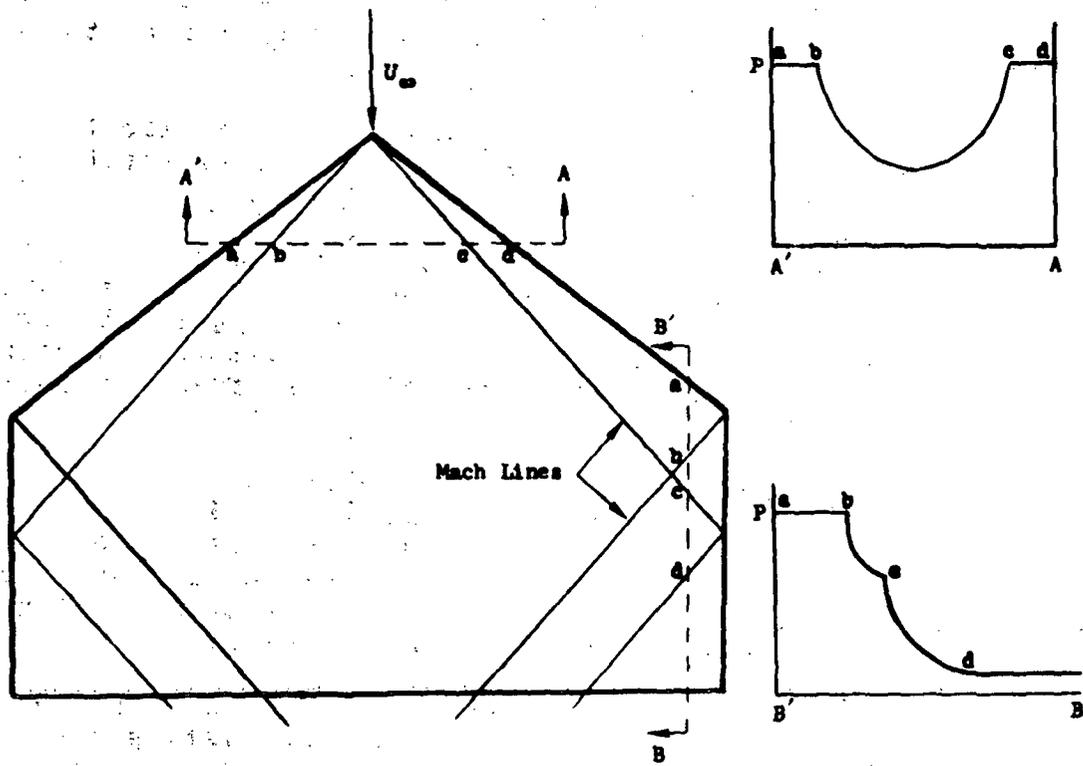
(a) Supersonic Leading Edge
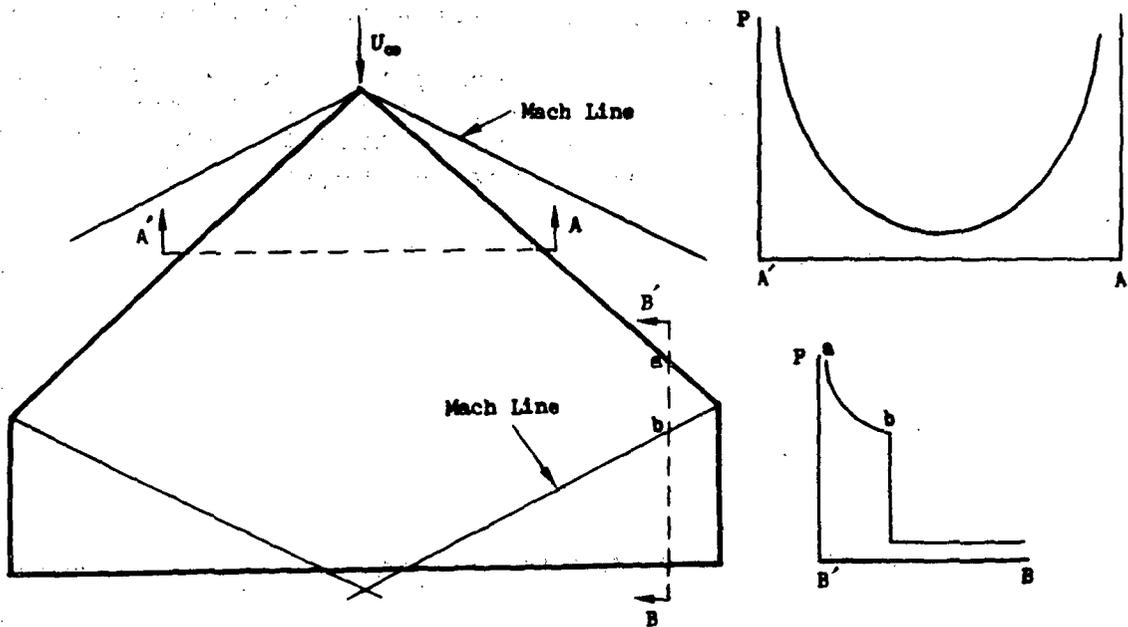
(b) Subsonic Leading Edges

FIGURE 1 - EDGE CONDITIONS FOR SUPERSONIC PLANFORMS

11

5.0 VORTEX SPLINE SCHEME

5.1 General Approach

As outlined in the introduction, most lifting surface schemes model flow problems by relating one flow parameter to another. For analysis problems the known parameter is the vehicle shape while the unknown is the pressure distribution. Since both the known and unknown parameters can be expressed in terms of velocity and velocity related parameters the forthcoming analysis will be derived using these variables.

Assuming linearized flow, the perturbation pressure can be expressed as:

$$\delta P = -\rho_\infty U_\infty \delta u \qquad (1)$$

where δu is the perturbation velocity in the free stream direction with U_∞ being the free stream velocity. Dividing Equation (1) by the dynamic pressure, $\frac{1}{2}\rho_\infty U_\infty^2$, gives:

$$\frac{\delta P}{\frac{1}{2}\rho_\infty U_\infty^2} = -2\frac{\delta u}{U_\infty} \qquad (2)$$

or

$$C_p = -2u \qquad (3)$$

where C_p is the pressure coefficient and $u = \delta u / U_\infty$ is a nondimensional perturbation velocity.

Across a lifting surface there is a jump in pressure, ΔC_p, corresponding to a jump in the perturbation velocity, u. This jump can be expressed in terms of another velocity related flow parameter - the bound vorticity, γ:

$$\gamma \equiv u_u - u_\ell \qquad (4)$$

where u_u is the upper surface velocity perturbation and u_ℓ is the lower surface velocity perturbation.

12

Since γ corresponds to an antisymmetric shear across the lifting surface (Ref. 5, pg. 129)

$$u_u = -u_\ell = u \qquad\qquad (5)$$

therefore:

$$\gamma = 2u \qquad\qquad (6)$$

and:

$$\Delta C_p = 2(u_u - u_\ell) = 4u = 2\gamma$$

$$(7)$$

From Equation (7) it is clear that the jump in pressure across a surface, assuming linearized flow, is directly related to the shear flow parameter - bound vorticity, γ .

On a two-dimensional planar surface, there are two components of velocity which are discontinuous, u and v; there are correspondingly two components of vorticity - γ corresponding to u and σ corresponding to v (see Ref. 6, pg. 221):

$$\sigma \equiv -(v_u - v_\ell) = -2v \qquad\qquad (8)$$

where v is the nondimensional, perturbation velocity normal to the free stream.

In treating potential flow, σ and γ are not independent and can be related through Helmholtz theorem (Ref. 6, pg. 221) as (Fig. 2):

$$\frac{\partial \sigma}{\partial x} + \frac{\partial \gamma}{\partial y} = 0 \qquad\qquad (9)$$

An elementary solution to the governing differential equation:

$$(1 - M^2) \frac{\partial^2 \phi}{\partial x^2} + \frac{\partial^2 \phi}{\partial y^2} + \frac{\partial^2 \phi}{\partial z^2} = 0 \qquad\qquad (10)$$

13
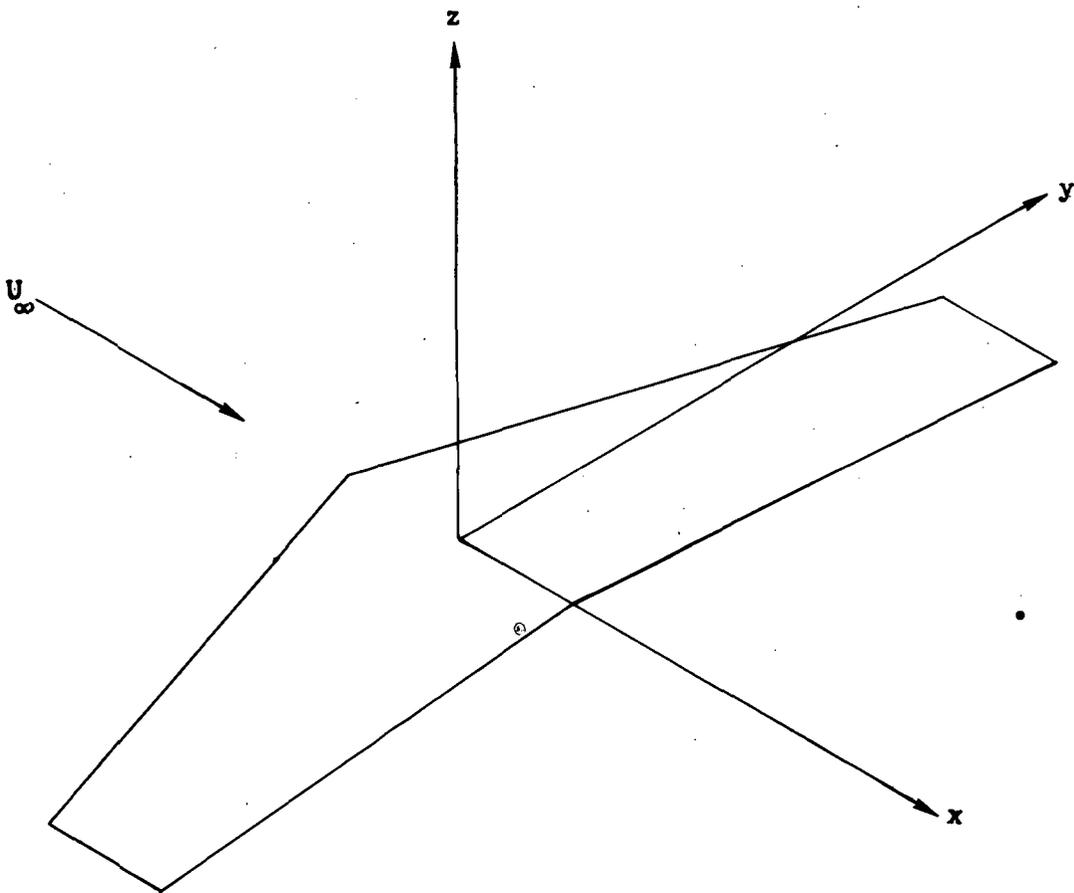
FIGURE 2 - AXIS SYSTEM FOR FLOW MODELING

14

which produces shear flow corresponding to vorticity can be obtained by integrating the basic doublet (Ref. 5). This solution termed the "elementary horseshoe vortex" automatically satisfies the linearized wake boundary condition of a jump in potential but no jump in pressure.

Using the elementary horseshoe vortex as the basic singularity, planar flow problems can be modeled as follows:

$$w(x,y) = \iint_s \gamma(\zeta,\eta) K(\zeta-x, \eta-y) d\zeta d\eta \qquad (11)$$

where $w(x,y)$ is the known nondimensional downwash velocity (for small angles w is approximately α, the angle of attack), x and y are field points, s is the region over which the singularities are distributed, $\gamma(\zeta,\eta)$ is the unknown bound vorticity distribution, and $K(\zeta-x, \eta-y)$ is the horseshoe vortex kernel function.

For subsonic flow, the region of influence, s, and the entire singularity surface coincide. The kernel function for this flow regime is (Ref. 5, pp. 87 and 149):

$$K(\zeta-x, \eta-y) = \frac{1}{4\pi} \frac{1}{(\eta-y)^2} \left[1 - \frac{\zeta-x}{\sqrt{(\zeta-x)^2 + \beta^2(\eta-y)^2}} \right] \qquad (12)$$

where $\beta^2 = 1 - M^2$.

For supersonic flow, the region of influence, s, is the portion of the singularity surface contained in the forward Mach cone emanating from the field point (x,y). The kernel function for this flow regime is derived in the same manner as was done for subsonic flow (Ref. 5, pg. 87) except that the analysis begins with the supersonic source (Ref. 5, pg. 88). Since the supersonic singularities can only influence locations within the aft Mach cone, the integration along the line of doublets does not range from x to ∞ but rather from x to the intersection of the line of doublets with the forward Mach cone from the influenced point (i.e., $x - \beta \sqrt{(\eta-y)^2}$ for a doublet line in the $z=0$ plane). The resulting kernel function is:

$$K(\zeta-x, \eta-y) = -\frac{1}{2\pi} \frac{1}{(\eta-y)^2} \frac{\zeta-x}{\sqrt{(\zeta-x)^2 - \beta^2(\eta-y)^2}} \qquad (13)$$

where β^2 is defined as M^2-1 for supersonic flow.

15

As mentioned earlier, $\gamma(\zeta,\eta)$, the unknown, can be represented in an approximate way as a series of basic distributions $\gamma_j(\zeta,\eta)$, so that:

$$\gamma(\zeta,\eta) = \sum_{j=1}^{N} S_j \, \gamma_j(\zeta,\eta) \tag{14}$$

where S_j is the strength of the jth distribution. This technique permits the integration to be performed using the known distributions of $\gamma_j(\zeta,\eta)$; thereby reducing the problem to an algebraic solution for S_j. The algebraic formulation is established by specifying the downwash at $M \geq N$ "control points" (i.e., collocation points):

$$w(x_i, y_i) = w_i \qquad i = 1, \dots M \tag{15}$$

where w_i is the downwash at x_i, y_i. Substituting Equation (14) into Equation (11) and integrating yields:

$$w_i = \sum_{j=1}^{N} A_{ij} S_j \qquad i = 1, \dots M \tag{16}$$

The aerodynamic influence coefficient, $A_{ij} = \dfrac{\partial w_i}{\partial S_j}$, represents the integral in Equation (11) (with S_j =1) and gives the downwash at point i due to unit strength of the jth distribution of vorticity. Equations (16) are a set of algebraic equation for S_j. For M equal to N, Equations (16) are a determinate set of algebraic expressions with a unique solution for the S_j. For M greater than N there are more equations than unknowns and, as will be shown later, the S_j can be determined in a least square error sense. Once the S_j are computed the pressures and pressure jumps can be computed from Equation (7).

Lifting surface schemes using the horseshoe vortex kernel, differ in the form of the basic distribution, $\gamma_j(\zeta,\eta)$ that they assume. They also differ in the manner in which the boundary conditions are satisfied, through the location of the field points and/or the number used in relation to the number of unknowns. The next section describes the type of vorticity assumed for the vortex spline scheme.

5.2 Selection of Vorticity Distribution

o Two-Dimensional Study

Before attempting a full three-dimensional study, various numerical techniques were first developed in two-dimensions. These two-dimensional studies supplied insight while at the same time providing a fundamentally simpler means to obtain numerical results than would be required for the full three-dimensional problem. The initial investigation concerned various vorticity distributions. In two dimensions, the basic vorticity kernel function for downwash is:

$$K(x) = \frac{1}{2\pi} \frac{1}{x-\zeta} \tag{17}$$

therefore the downwash is:

$$w(x) = \frac{1}{2\pi} \int_{x_1}^{x_2} \frac{\gamma(\zeta)}{x-\zeta} d\zeta \tag{18}$$

A study was made using this expression as a two-dimensional formulation of the constant pressure panel scheme. With $\gamma(\zeta)=1$ for $x_1 < \zeta < x_2$ the integration can then be performed yielding:

$$w(x) = \frac{1}{2\pi} \ln\left|\frac{x-x_1}{x-x_2}\right| \tag{19}$$

Figure 3 shows how the scheme is used to model the loading on a flat plate at angle of attack.

The vorticity distribution is a series of step functions. The influence of the jth step function, having strength, S_j, on the ith control point can be expressed from Equation (19) as:

$$w(x_i)_j = w_{ij} = \frac{1}{2\pi} S_j \ln\left|\frac{x_i - x_j}{x_i - x_{j+1}}\right| \tag{20}$$

or

$$w_i = A_{ij} S_j \tag{21}$$
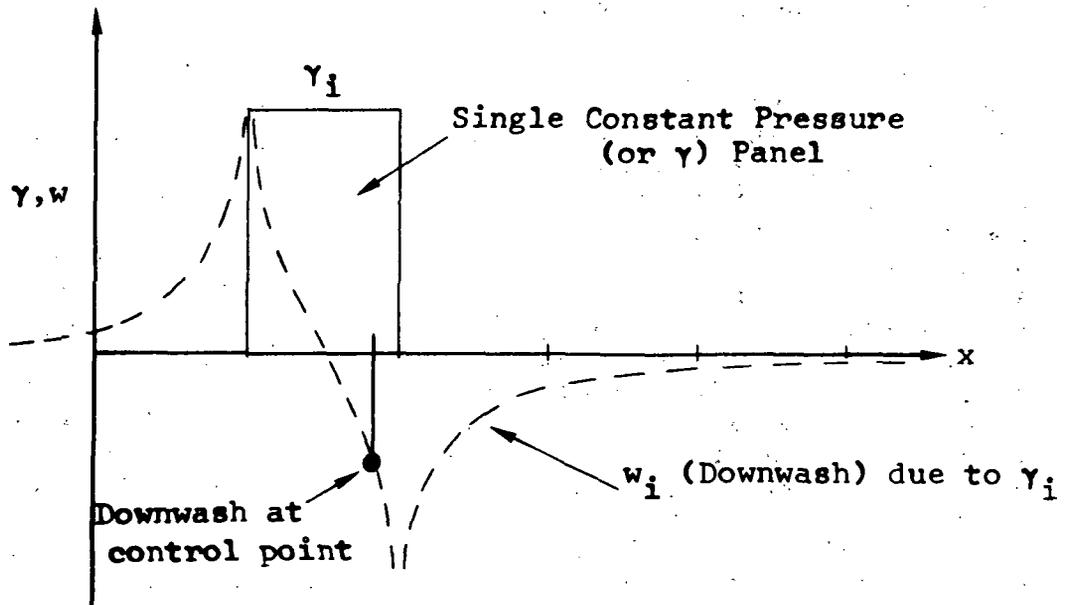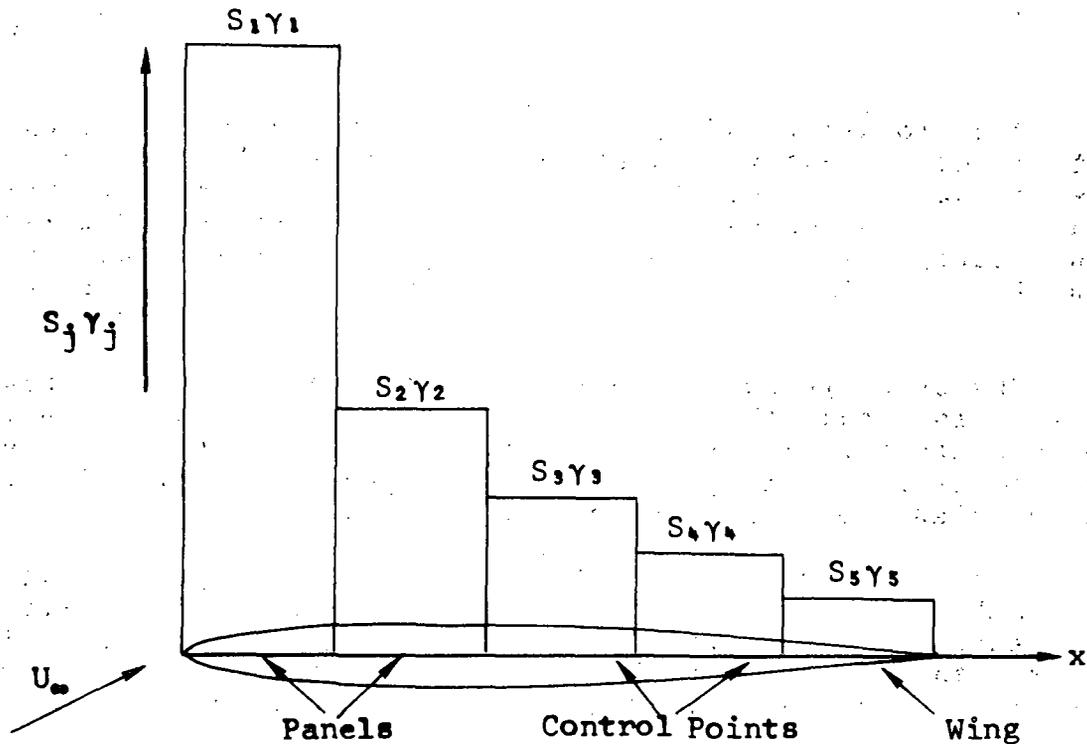
FIGURE 3 - CONSTANT PRESSURE PANEL SCHEME IN TWO DIMENSIONS

where

$$A_{ij} = \frac{1}{2\pi} \ln\left|\frac{x_i - x_j}{x_i - x_{j+1}}\right|$$

(22)

The location of the control points is computationally determined so that the numerical results will be correct over a wide range of problems. Since there is one control point and one value of S_j corresponding to each panel, Equations (16) constitute a determinate set of linear algebraic equations (M=N) which can easily be solved for the strengths S_j.

The thing to note about the constant pressure panel scheme is that the downwash field for the panels contain a logarithmic singularity at each panel edge. This means that the control point placement on the panel is critical since the gradients of the downwash can be large.

Figure 4 shows the results of the flat plate analysis for subsonic flow. These results show the large downwash gradients and also show that there is no way to specifically invoke the Kutta condition at the trailing edge. This condition is implied through the control point location.

In spite of these problems the results are fairly good; but, however, they are not sufficient for the interaction problem (as pointed out in the introduction).

In order to improve upon these results it was apparent that two things had to be done - 1) remove as many of these logarithmic singularities as practical, and 2) establish some definite means to introduce the Kutta condition in subsonic flow. The first item was achieved by noting that the logarithmic singularities arise from jumps in the vorticity strength therefore a new distribution had to be formulated which had continuity of vorticity level. This implied that the vorticity had to posess at least a linear variation (consistent with the requirements set forth in Ref. 4, and outlined in the Introduction). There are two means to obtain a continuous distribution using a linear distribution - one is to place separate continuity constraints on the solution across panel edges using a method such as Lagrangian multipliers; the other is to form the functions so that they automatically provide continuous distributions. This second means was selected because of the inherent simplicity in the mathematical formulation. Figure 5 shows the basic function used for the new two-dimensional numerical scheme. This figure also implies that there is still a jump in the

19
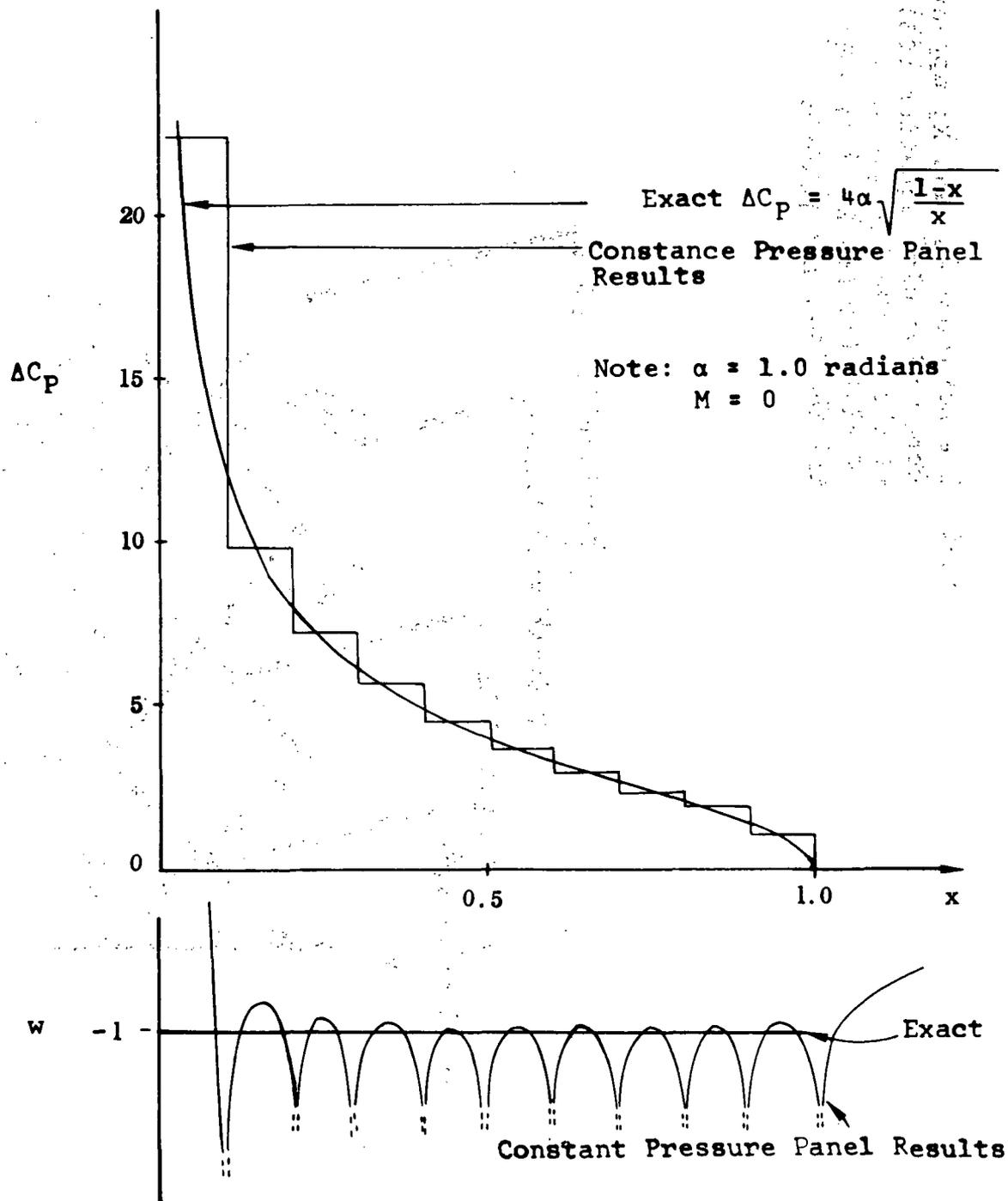
FIGURE 4 - TWO DIMENSIONAL CONSTANT PRESSURE PANEL RESULTS

Note: The notation X_i^1 and X_i^2 appears in conjuction with equation (25) and refers to the two chordwise segments of distribution X_i. (The superscripts are indices, not powers.)

Distribution 1, X_1

Distribution 2, X_2

Distribution 3, X_3

Distribution 4, X_4

X_3^1

X_3^2

Y

1

X

Panel 1

Panel 2

Panel 3

x_{LE} for X_3^1

x_{LE} for X_3^1

x_{TE} for X_3^1

x_{LE} for X_3^2

x_{TE} for X_3^2
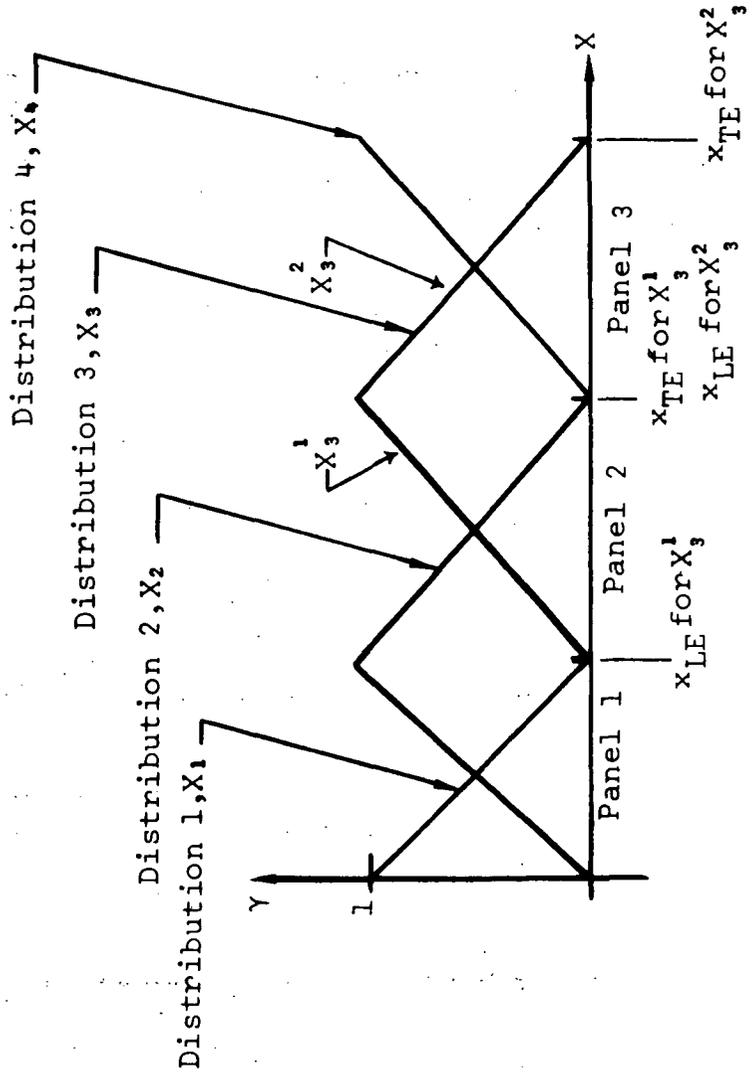
FIGURE 5 - LINEAR VORTICITY REPRESENTATION USED CHORDWISE

vorticity at the leading edge which causes a logarithmic singularity. The only way to remove this singularity at the leading edge is to use the proper asymptotic form which is related to the reciprical of the square root of the distance from the edge (Figure 4). The new scheme was tested with and without the proper singular form, the conclusion was that there was sufficient accuracy for lift and moment without this singular variation in the vorticity.

Figure 5 shows that the triangular distribution of vorticity provides a natural means of introducing the Kutta condition by omitting the last function. This omission forces the vorticity to vanish at the trailing edge.

The vortex spline formulation is based on a different means of satistying the boundary conditions which will be discussed later; but the fundamental approach is to compute the downwash at discrete locations using the basic triangular distributions of vorticity, γ , in Equation (18) with the limits changed to include two panels per distribution (Figure 5). Figure 6 shows the results for subsonic flow.

o Basic Three-Dimensional Function

For the three dimensional formulation of the scheme, two components of vorticity must be considered, γ and σ . As pointed out earlier, these two components are not independent in potential flow. This means that it is not possible to arbitraily legislate that both components vary linearly in all directions. Using Equation (9) to solve for σ in terms of γ gives:

$$\sigma = -\frac{\partial}{\partial y} \int \gamma \, dx \qquad (23)$$

From the two-dimensional study where γ was the only component present, the variation streamwise (x) needed to avoid logarithmic singularities was linear. Equation (23) then states that σ must vary quadratically in x. This same analysis can be repeated using the other requirement that σ vary linearly normal to the stream (y) in order to eliminate singularities. Solving Equation (9), this time for γ , yields:

$$\gamma = -\frac{\partial}{\partial x} \int \sigma \, dy \qquad (24)$$

This means that γ must vary quadratically in y.

22
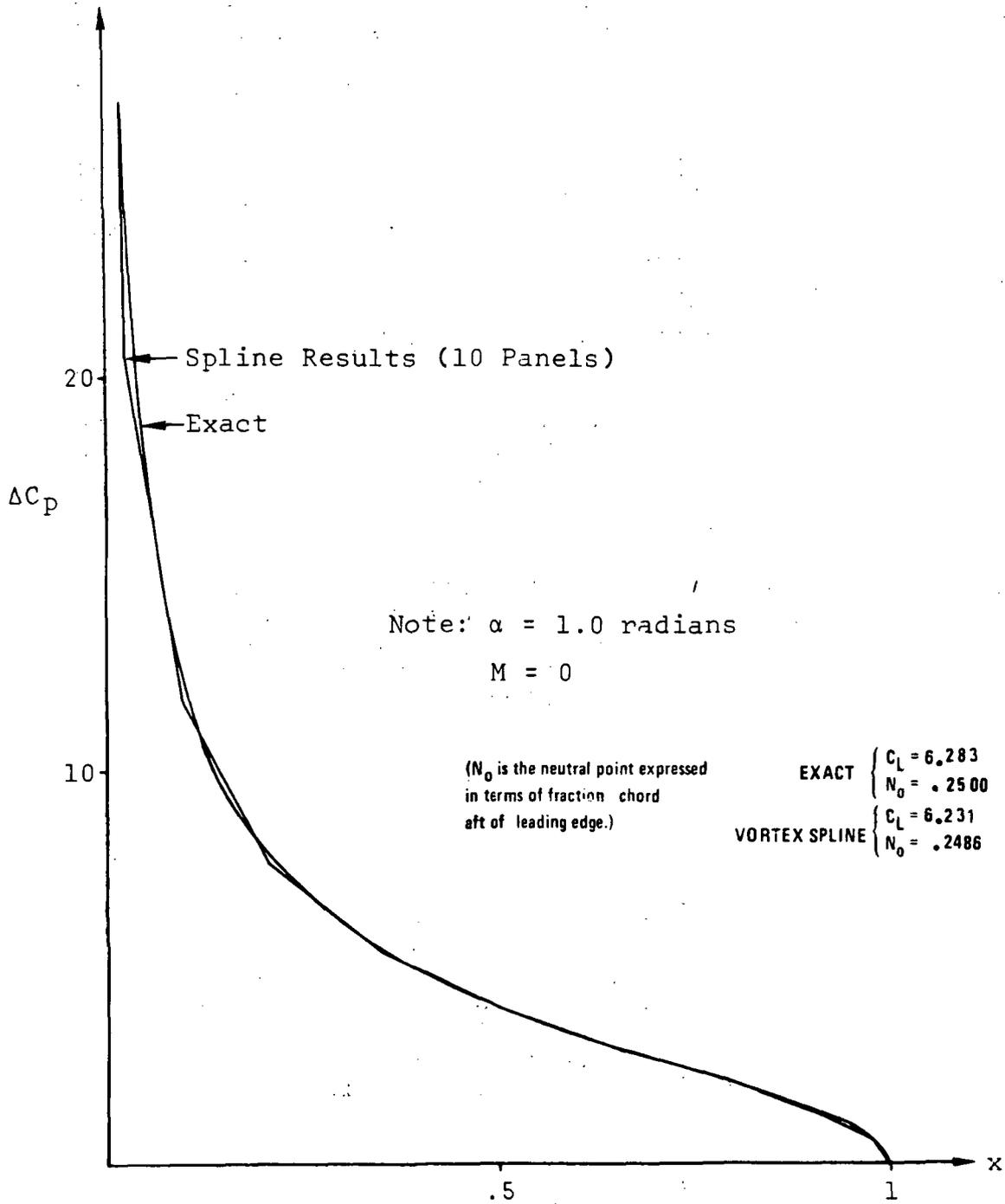
FIGURE 6 - TWO DIMENSIONAL SPLINE RESULTS

23

Summarizing then:
γ - linear in x, quadratic in y
σ - linear in y, quadratic in x

(A plot of σ versus y would be analogous to Figure 5-a series of linear functions.)

With this above variation the only places where singularities would occur on a simple rectangular wing would be at the leading edge (due to a jump in γ) and at the tips (due to a jump in σ) for subsonic flow and at the tips only for supersonic flow (Figure 7).

Since the elementary horseshoe vortex is best described in terms of γ , the criteria established above for this component of vorticity was the one used as the basis to derive the three dimensional distribution function presented next.

For the x variation of γ in three-dimensions, the requirement shown above is the same as that for two-dimensions. However, the y variation has to be quadratic or, in more fundamental terms, continuous in both value and slope in order for σ to be continuous in value. The logical means to form such a surface distribution seemed to be as a product of two functions - one providing the desired linear x variation and another providing the desired quadratic y variation. To see how this y variation was formed, consider the basic triangular form used in two-dimensions. This distribution has, in general, three discontinuities in slope. By adding three discontinuous quadratic distributions to this basic form, these discontinuities can be removed. Figure 8 shows how this is accomplished. The requirement for each of the quadratic functions is that they begin and end at the centers of panels (spanwise) with zero value and slope, and also have a discontinuity in slope at the panel edge which cancels the discontinuity in slope of the triangular function. The overall function then becomes six separate quadratics which cover four panels spanwise. The equations of these quadratics can be computed from the imposed boundary conditions on each segment. Table 1 gives these results. (As a note, these spanwise functions could have also been developed using three quadratics over three panels specifying the slope and value matches at the two inner panel edges, and also requiring the distribution to vanish in both value and slope at the outside edges. The additional requirement of unit maximum value would then completely specify the distribution.)

24

U_∞

Downwash singularities along these edges only.
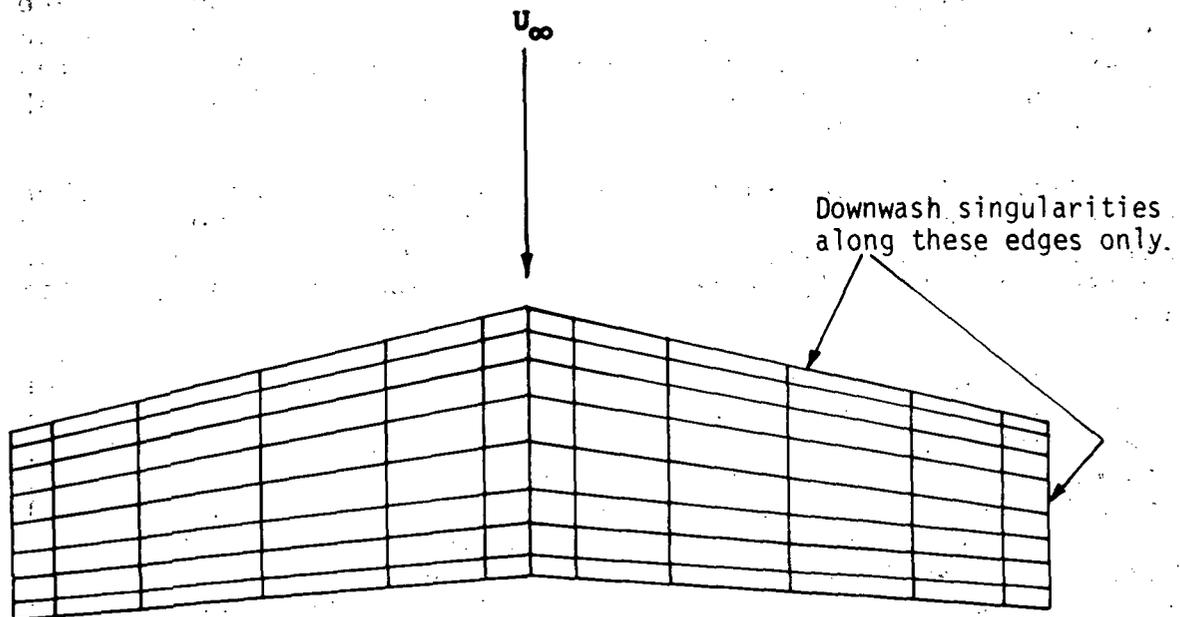
Note: no downwash singularity at leading edge, if edge is supersonic

FIGURE 7 - LOCATION OF DOWNWASH SINGULARITIES WITH VORTEX SPLINE
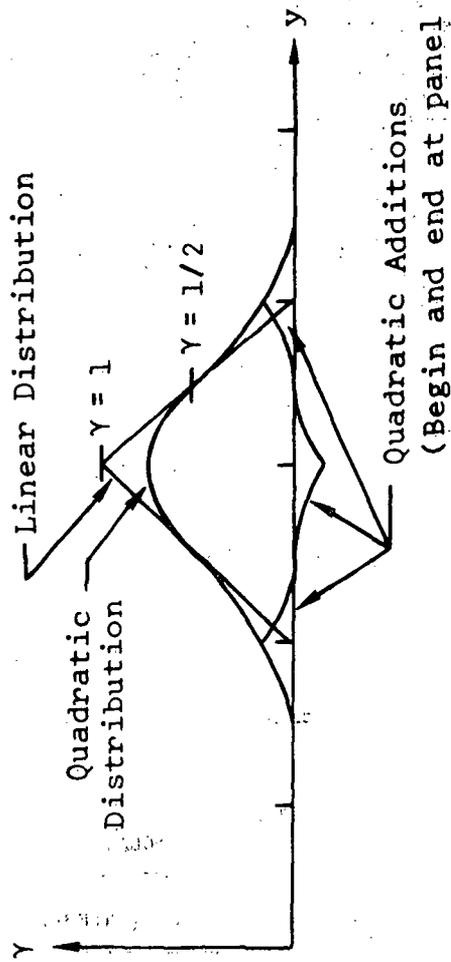
FIGURE 8 - QUADRATIC DISTRIBUTION FORMED FROM LINEAR FUNCTION AND QUADRATIC ADDITIONS

26

$$Y^n = A_n + B_n \bar{y} + C_n \bar{y}^2$$

($\bar{y}$ ranges from 0 to 1 on each panel, ℓ_n)

Segment (n)	Boundary Conditions*		Constants		
	Left Edge	Right Edge	A_n	B_n	C_n
1	$Y^1 = 0$ $\dot{Y}^1 = 0$	$Y^1 = Y^2$ $\dot{Y}^1 = Y^2$	$\dfrac{\frac{1}{4}\ell_1}{\ell_1 + \ell_2}$	$\dfrac{-\ell_1}{\ell_1 + \ell_2}$	$\dfrac{\ell_1}{\ell_1 + \ell_2}$
2	$Y^2 = Y^1$ $\dot{Y}^2 = \dot{Y}^1$	$Y^2 = \frac{1}{2}$ $\dot{Y}^2 = 1/\ell_2$	$\dfrac{\frac{1}{4}\ell_1}{\ell_1 + \ell_2}$	$\dfrac{\ell_2}{\ell_1 + \ell_2}$	$\dfrac{\ell_1}{\ell_1 + \ell_2}$
3	$Y^3 = \frac{1}{2}$ $\dot{Y}^3 = 1/\ell_2$	$Y^3 = Y^4$ $\dot{Y}^3 = \dot{Y}^4$	$-\dfrac{1}{4}$	2	-1
4	$Y^4 = Y^3$ $\dot{Y}^4 = \dot{Y}^3$	$Y^4 = \frac{1}{2}$ $\dot{Y}^4 = -1/\ell_3$	$\dfrac{3}{4}$	0	-1
5	$Y^5 = \frac{1}{2}$ $\dot{Y}^5 = -1/\ell_3$	$Y^5 = Y^6$ $\dot{Y}^5 = Y^6$	$\dfrac{\ell_3 + \frac{3}{4}\ell_4}{\ell_3 + \ell_4}$	$-\dfrac{\ell_3 + 2\ell_4}{\ell_3 + \ell_4}$	$\dfrac{\ell_4}{\ell_3 + \ell_4}$
6	$Y^6 = Y^5$ $\dot{Y}^6 = \dot{Y}^5$	$Y^6 = 0$ $\dot{Y}^6 = 0$	$\dfrac{\frac{1}{4}\ell_4}{\ell_3 + \ell_4}$	$-\dfrac{\ell_4}{\ell_3 + \ell_4}$	$\dfrac{\ell_4}{\ell_3 + \ell_4}$

*Note: Left edge of the odd numbered panels begins at $\bar{y} = \frac{1}{2}$; $\dot{Y}^n = \frac{dY^n}{dy}$

TABLE 1 – COEFFICIENTS OF SPANWISE VARIATION

If X_i is used to represent the chordwise variation of γ_k and Y_j is used to represent the spanwise variation of γ_k, the distribution of vorticity could be expressed as a doubly subscripted variable, $\gamma_{i,j}$. However, in order to conform with the singly subscripted γ_k of Equation (14), a unique relationship between k and i,j was assigned so that:

$$\gamma_k = \gamma_{i,j} = X_i\, Y_j \qquad k = 1 \ldots N \qquad (25)$$

where Y_j consists of the six quadratic segments Y_j^n (n = 1,2,...,6) shown in Table 1 and X_i consists of the two linear segments X_i^m (m = 1,2) shown in Figure 5. Thus, the analytic description of $\gamma_k = \gamma_{i,j}$ consists of twelve discrete parts, $X_i^m\, Y_j^n$ (m = 1,2; n = 1,2,...,6). These parts are distributed over eight panels (four spanwise, two chordwise) as shown in Figure 9.

For a set of rectangular panels, X_i is only a function of the streamwise coordinate, x. By definition, Y_j is only a function of y, providing the spanwise edges are aligned with the free stream (which by the panel definitions, will always be the case). If the panels are not rectangular, X_i becomes a function of both x and y so that it varies as the fraction of local chord:

$$X_i^1 = \frac{x - x_{LE}}{x_{TE} - x_{LE}} \qquad (26)$$

and

$$X_i^2 = \frac{x_{TE} - x}{x_{TE} - x_{LE}} \qquad (27)$$

In the above equations, x_{LE} and x_{TE} are the leading and trailing edge coordinates of the panel covered by segment X_i^1 (X_i^2); this is illustrated in Figure 5.

Except for rectangular panels, X_i^1 and X_i^2 will be functions of y. If the fraction of local chord is defined as:

$$\bar{x} = \frac{x - x_{LE}}{x_{TE} - x_{LE}} \qquad (28)$$

then X_i becomes

28

FIGURE 9 - SURFACE SPLINE DISTRIBUTION OF VORTICITY

Segments of X_i

X_i^2

X_i^1

Y_j^6

Y_j^5

Y_j^4

Y_j^3

Y_j^2

Y_j^1

$\gamma_{i,j} = X_i Y_j$

Segments of Y_j

Y

X

$\gamma_{i,j}$

29
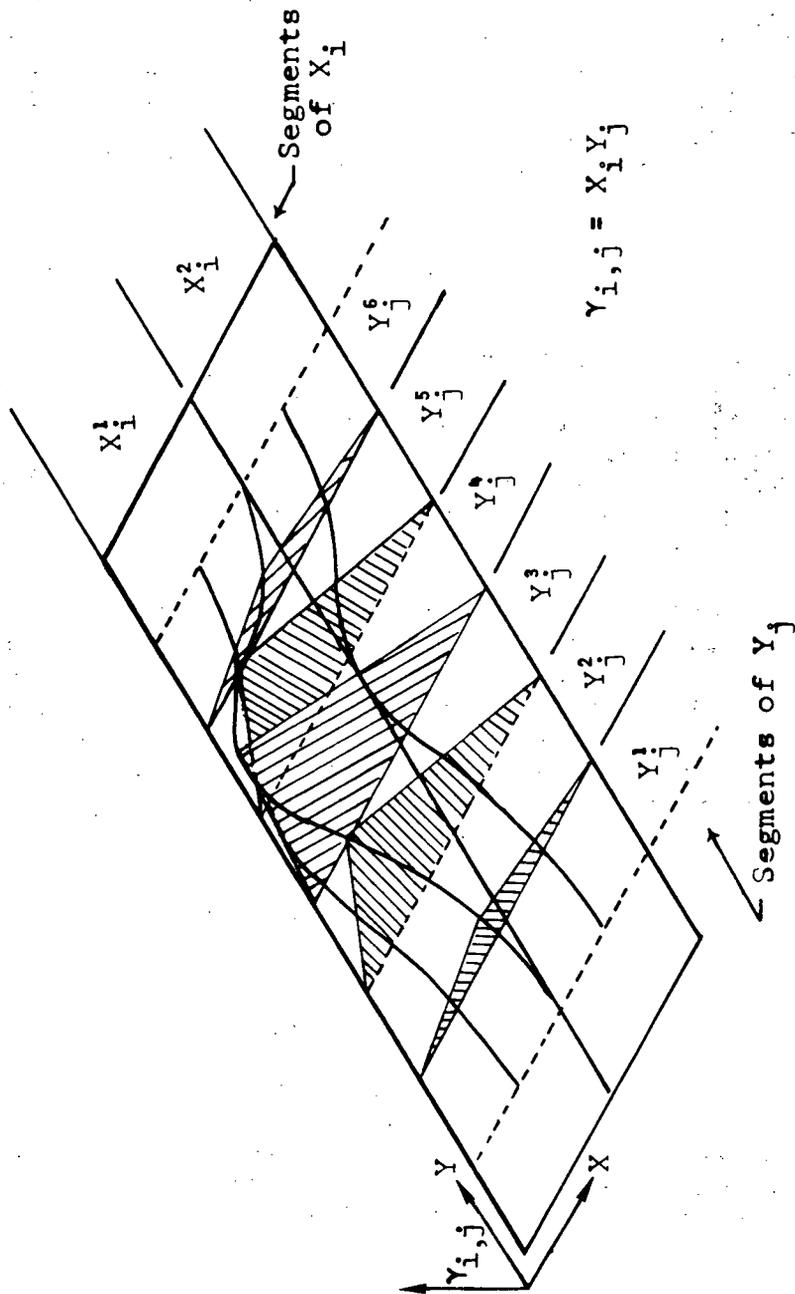
$$X_1^1 = \bar{x} \qquad (29)$$

and

$$X_1^2 = 1 - \bar{x}$$

$$(30)$$

The above representation holds for all leading and trailing, panel edge shapes.

The bound vorticity distribution defined by Equation (25) (termed spline) and shown in Figure 9, produces no singularities in the downwash. This function is scaled up and down in the solution exactly the same way as the constant pressure panel scheme using a multiplicative constant which is the unknown.

The next sections describe how a wing is subdivided into panels and how the basic splines are overlapped using these subdivisions.

o Modeling Vorticity on a Wing Using Vorticity Splines

Figure 10 shows a paneled wing with both a spanwise cut and a chordwise cut to display the chordwise and spanwise overlapping of the basic spline functions (assuming unit amplitude). For the five chordwise functions and the six spanwise functions shown, there will be a total of thirty (N=30) spline functions distributed over twenty-five wing panels. The components of a single function are identified (shaded area) to depict its relationship to the overall arrangement. This figure also shows that the Kutta condition has been imposed (zero value of function at trailing edge).

As shown in Table 2, special functions are used at the root and tip, the functions for symmetric flow will be discussed first.

The first root function (root function 1) is the right half (spanwise) of a normal function. The second root function (root function 2) is composed of segments Y^3, Y^4, Y^5 and Y^6 of a normal function with Y^6 of the corresponding function on the left half of the wing added to Y^2 of the right side function. Adding these two terms accounts for the overlapping of the right and left halves. (This can be done since the magnitude of function

30

Shaded area represents the extent of function $Y_k = Y_{3,3} = X_3 Y_3$

Area covered by $X_3^1 Y_3^6$

Area covered by $X_3^2 Y_3^1$

U_∞

Remove for Kutta Condition

(Tip Function 1)

(Tip Function 2)
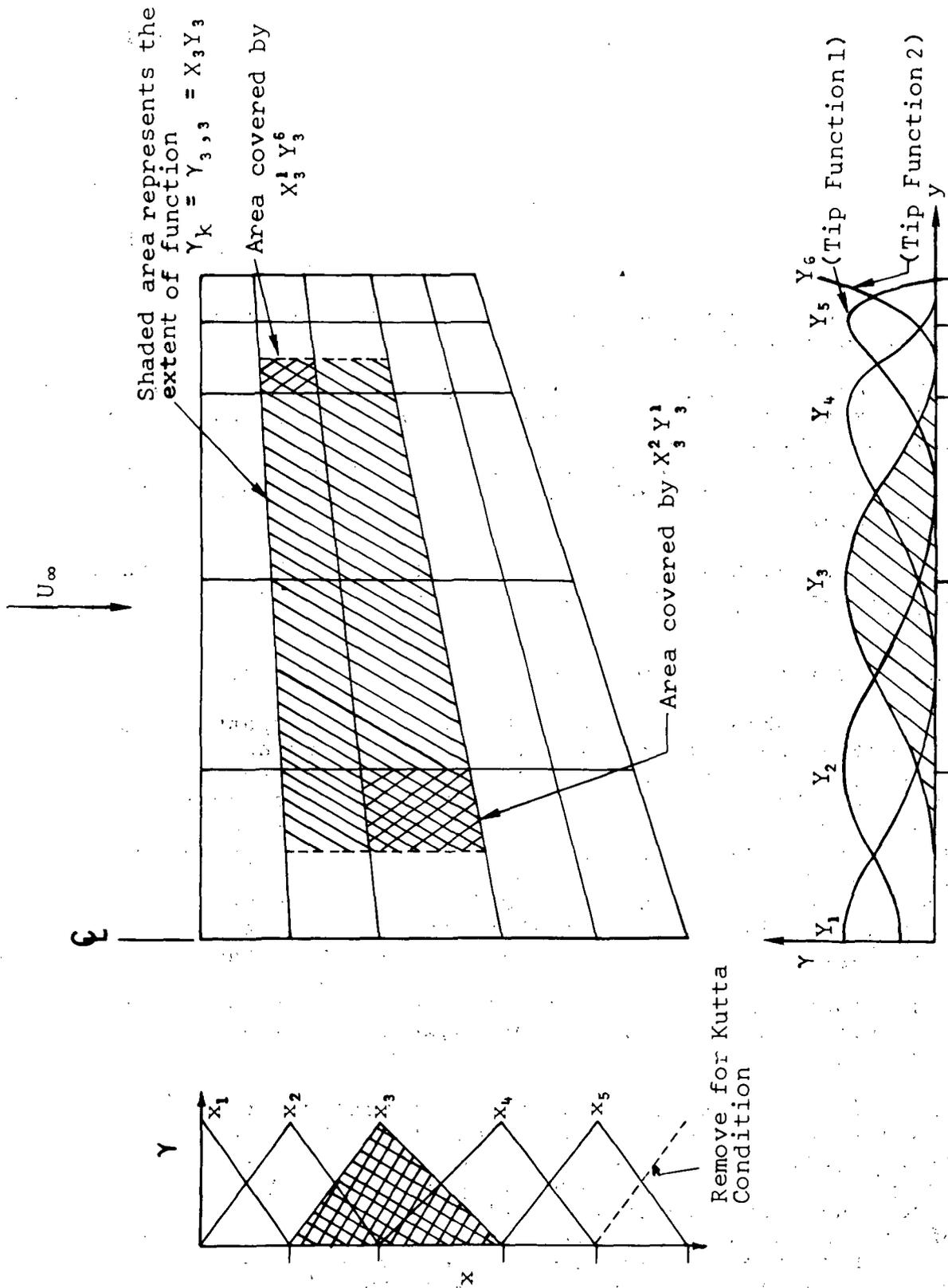
FIGURE 10 — SPLINE FUNCTIONS DISTRIBUTED ON A WING (SYMMETRIC FLOW)

31

Root Function -·Symmetric

$$Y^n = A_n + B_n\bar{y} + C_n\bar{y}^2$$

($\bar{y}$ ranges from 0 to 1
on each panel, ℓ_n)
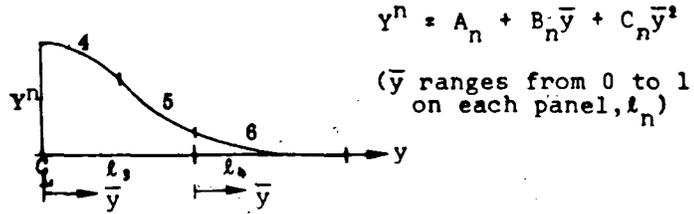
Segment (n)	Boundary Conditions		Constants		
	Left Edge	Right Edge	A_n	B_n	C_n
1 - 3	Do not	exist	—	—	—
4 - 6	Normal	Functions			

Note: The normal function represented by segments 4 through 6 at the root meets the proper symmetry requirement of vanishing slope.

Root Function 1 - Antisymmetric

Segments 1 through 6 do not exist

Root Function 2 - Symmetric

Normal Y^2 segment
Y^6 Function segment
from left side
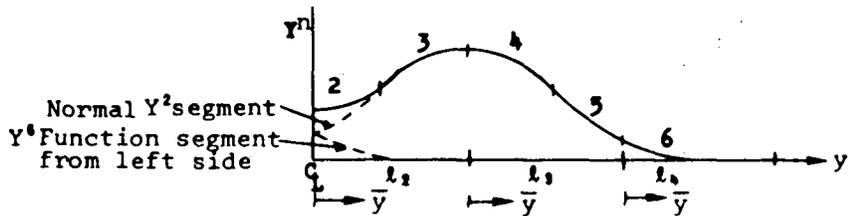
Segment (n)	Boundary Conditions		Constants		
	Left Edge	Right Edge	A_n	B_n	C_n
1	Does not exist		—	—	—
2	Combine functions	overlapping at the root	1/4	0	1
3-6	Normal	functions			

TABLE 2 - SPECIAL SPANWISE FUNCTIONS

Root Function 2 - Antisymmetric

Note: 2 & 3 are combined into one segment
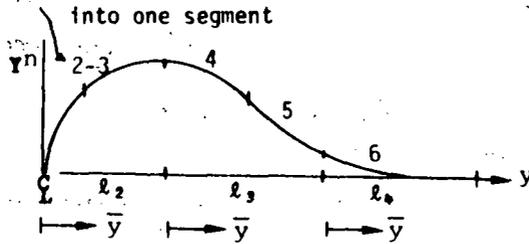
Segment (n)	Boundary Conditions		Constants		
	Left Edge	Right Edge	A_n	B_n	C_n
1	Does	not exist	—	—	—
2-3	$Y^{2-3} = 0$	$Y^{2-3} = Y^4$ $\dot{Y}^{2-3} = \dot{Y}^4$	0	3/2	-3/4
4-6	Normal	functions			

Tip Function - 1
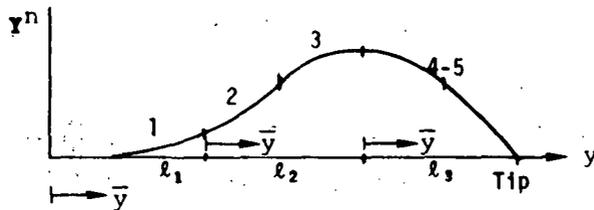
Segment (n)	Boundary Conditions		Constants		
	Left Edge	Right Edge	A_n	B_n	C_n
	Normal	functions			
4-5	$Y^{4-5} = Y^3$ $\dot{Y}^{4-5} = \dot{Y}^3$	$Y^{4-5} = 0$	3/4	0	-3/4
6	does	not exist	—	—	—

TABLE 2 - CONTINUED

Tip Function - 2
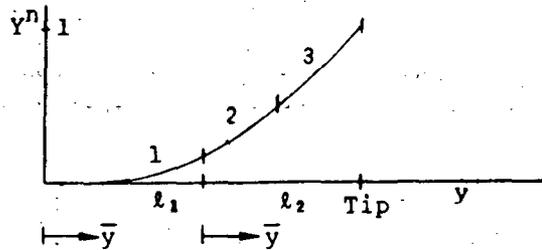
Segment (n)	Boundary Conditions		Constants		
	Left Edge	Right Edge	A_n	B_n	C_n
1	Normal	function			
2 *	$Y^2 = Y^1$ $\dot{Y}^2 = \dot{Y}^1$	$Y^2 = Y^3$ $\dot{Y}^2 = \dot{Y}^3$	$1/4 \; \dfrac{\ell_1}{\ell_1 + \ell_2}$	$\dfrac{\ell_2}{\ell_1 + \ell_2}$	$\dfrac{3/4 \; \ell_1 - 1/4 \; \ell_2}{\ell_1 + \ell_2}$
3 *	$Y^3 = Y^2$ $\dot{Y}^3 = \dot{Y}^2$	—	1/4	0	3/4
4 - 6	Do	not exist	—	—	—

* Note: An additional constraint was placed on segment 2 and 3 which required that the combined spanwise distributions be capable of representing a constant

TABLE 2 - CONCLUDED

corresponding to the γ^6 segment is the same as that corresponding to the γ^2 segment-by symmetry. The reason for this treatment will be explained in the next section.)

The next to last tip function (tip function 1) has γ^1, γ^2, and γ^3 as normal segments. γ^6 does not exist; γ^4 and γ^5 are one continuous quadratic function, the boundary conditions of which are: 1) continuous slope and value at left edge of the tip panel, and 2) zero value at the tip.

The last tip function (tip function 2) has γ^1 as a normal segment, but γ^2 and γ^3, the only remaining segments, are determined such that when this tip function is added to the other functions, the combination will produce a constant value of γ if all the strengths (multiplicative coefficients) are the same. This requirement was set because, in supersonic flow, the vorticity strength can be constant approaching a pointed tip. This tip distribution modeling capability also tended to yield the best numerical results of any of the variations studied (for both subsonic and supersonic flows).

For antisymmetric flow (e.g., rolling) the root functions have to be altered. Figure 11 shows these modified spanwise variations. The first root function (Y_1) has been deleted. The most inboard function (Y_2), for the antisymmetric case, is the same as a reflection of the next to last tip function (Y_6). The remaining functions across the span are the same as for the symmetric case.

Table 2 gives all the coefficients for the special functions just described.

Figure 12 shows an example of how two functions are overlapped - that is share common panels. This illustration depicts one of the many possible ways that overlapping can occur.

Arbitrary flow problems involving symmetric configurations can be decomposed into a symmetric and an antisymmetric flow problem. In this way, only one half of the wing need be treated for each of these reduced problems. For symmetric flow, the unknown strengths have the same values for corresponding functions on opposite sides of the configuration's plane of symmetry. For antisymmetric flow, the strengths have the same magnitude but opposite sign for corresponding functions. Using these properties to formulate the problem results in the concept of real and image relations and the satisfaction of boundary conditions on one side of the plane of symmetry only (the other side
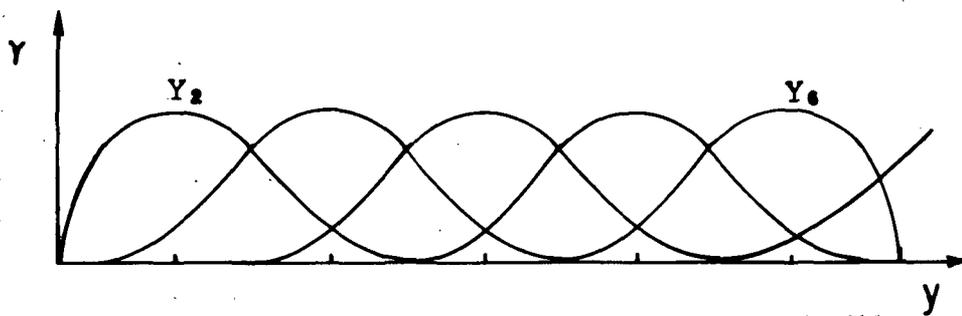
FIGURE 11 - ANTISYMMETRIC SPANWISE SPLINE DISTRIBUTION
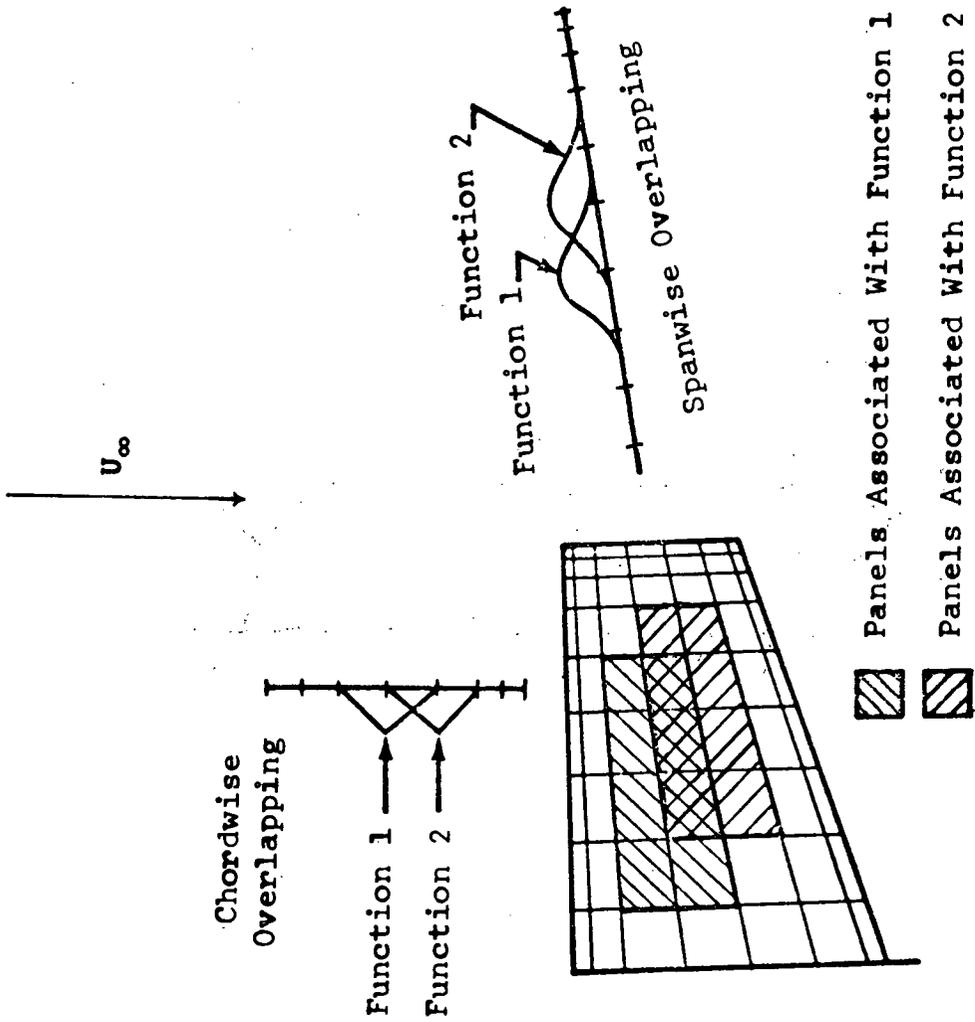
FIGURE 12 – OVERLAPPING OF SURFACE DISTRIBUTIONS

automatically satisfied by the appropriate symmetry relation). The symmetric problem is constructed as the sum of the influences from the real and image functions, where real and image implies corresponding functions on opposite sides of the symmetry plane. The antisymmetric problem is constructed as the difference of the influences from the real and image functions. This scheme reduces the number of calculations to be performed by half.

o Wing Paneling

As mentioned earlier, the basic paneling procedure is to cut the wing streamwise to form panels so that two panel edges are parallel to the free stream. This arrangement allows the kernel function integration to be performed more readily by introducing simple limits; it also simplifies the expression for the Y variation of the basic vorticity distribution (making it a function of y only).

The initial assumption for paneling was that the new technique use the same trapezoidal paneling as the constant pressure panel method (Ref. 1). Quickly, it was realized that any non-rectangular planforms would have discontinuities in the slopes of the fore and aft panel edges. Such discontinuities would introduce logarithmic singularities in the downwash field, including the wake. The source of these singularities can be seen by inserting the expression for the Y spline distribution (Eq. 25) into Equation (23).

$$\sigma(x, y) = -\frac{\partial}{\partial y} \int_{x_{LE}(y)}^{x_{TE}(y),x} X(\zeta, y) Y(y)\, d\zeta \qquad (31)$$

The upper limit of the above integral depends on whether σ is computed on the distribution (limit equal x) or behind the distribution (limit equal $x_{TE}(y)$).

The above equation shows that if any of the variables $Y(y)$, $X(x,y)$, $x_{LE}(y)$ or $x_{TE}(y)$ has a discontinuity in slope with respect to y then σ will be discontinuous in value – producing the logarithmic singularity. Of course $Y(y)$ is generated so that it is continuous in both value and slope so will not be of concern. This shows that planform breaks, which cause jumps in panel slopes, will produce the undesirable downwash singularities.

A method was developed to eliminate this problem by eliminating the planform breaks. Figure 13 shows the procedure and gives the resulting equations for the planform edges. The procedure shown is exactly the same one used to

38

Δ Slope quadratic $= \dfrac{d\Delta x_2}{dy}\Big|_{\overline{y}_2=1} - \dfrac{d\Delta x_1}{dy}\Big|_{\overline{y}_1=0} = -\dfrac{a}{\ell_2} - \dfrac{a}{\ell_1} = -a\left(\dfrac{\ell_1+\ell_2}{\ell_1\ell_2}\right)$

Δ Slope quadratic $= -\Delta$ Slope panel edge

$-a\left(\dfrac{\ell_1+\ell_2}{\ell_1\ell_2}\right) = -\left(\left(\dfrac{dx}{dy}\right)_2 - \left(\dfrac{dx}{dy}\right)_1\right)$

$a = \left(\dfrac{dx}{dy}\Big|_2 - \dfrac{dx}{dy}\Big|_1\right)\dfrac{\ell_1\ell_2}{\ell_1+\ell_2}$

● At the root the jump in slope is $2\dfrac{dx}{dy}$

● For the outer half of the tip panel no quadratic addition is employed

(b) Details of Quadratic Addition at Planform Breaks

$Y = X(x,y)\ Y(y)$

$\sigma(x,y) = -\dfrac{\partial}{\partial y}\displaystyle\int_{x_{LE}}^{x\ or\ x_{TE}(y)} Y dx$

$= -\dfrac{\partial}{\partial y}\displaystyle\int_{x_{LE}}^{x\ or\ x_{TE}(y)} X(x,y)Y(y)dx$

(a) Planform Break Treatment

FIGURE 13 – QUADRATIC PANEL REPRESENTATION ALONG A PLANFORM BREAK

39

change the basic, linear distribution of vorticity into the quadratic distribution (Figure 8).

An additional benefit of going to the quadratic edge panels is that they provide a more general modeling element to handle arbitrary planforms. Later results in this report will show their usefulness in modeling a circular wing.

The basic panel then is one with two parallel, streamwise edges with two quadratic edges; the quadratic changes coefficients at mid span. With this paneling arrangement there will be no downwash singularities in the wake (except from the tip)) and therefore, meets the desired requirement. (The quadratic paneling could also have been developed using one continuous quadratic across each panel edge in order to be compatible with the three spanwise panel developments mentioned earlier.)

The paneling described above is the one always used in subsonic flow. For supersonic flow, however, there are two choices of paneling - the one just described and another termed "special Mach line paneling." In this latter procedure certain Mach lines are identified, across which the vorticity level and/or gradient can be discontinuous (see Figure 1). These lines eminate from planform breaks, tips, etc. Along these lines continuity conditions can be relaxed and downstream sections can be treated as separate wings in the wake of the upstream sections. Interior to each section, the paneling is treated as though that section were a separate subsonic wing (normal quadratic panels), so that the γ_j distributions for each subdivision do not overlap panels of an adjacent subdivision.

Figure 14 shows a square wing at M equal $\sqrt{2}$ comparing the normal geometric paneling with the special Mach line paneling. Note that the planform breaks are eliminated even when they are due to the special Mach lines. Also note that since there are no singularities in the wakes emanating from each subdivision, the paneling of the subdivisions can be independent (except at planform breaks where the edges have to be aligned to ensure that the quadratic edges fore and aft coincide).

Numerical results computed with the special Mach line paneling (presented later in this report) show that this procedure greatly improves the details of the pressure distribution and at the same time allows for even greater variation in paneling options then afforded by the normal geometric paneling.

40

U_∞

Special Mach Line Paneling

Subdivision I

Subdivision II

Subdivision III

Curved Panel Edge

Special Mach Lines

Geometric Paneling
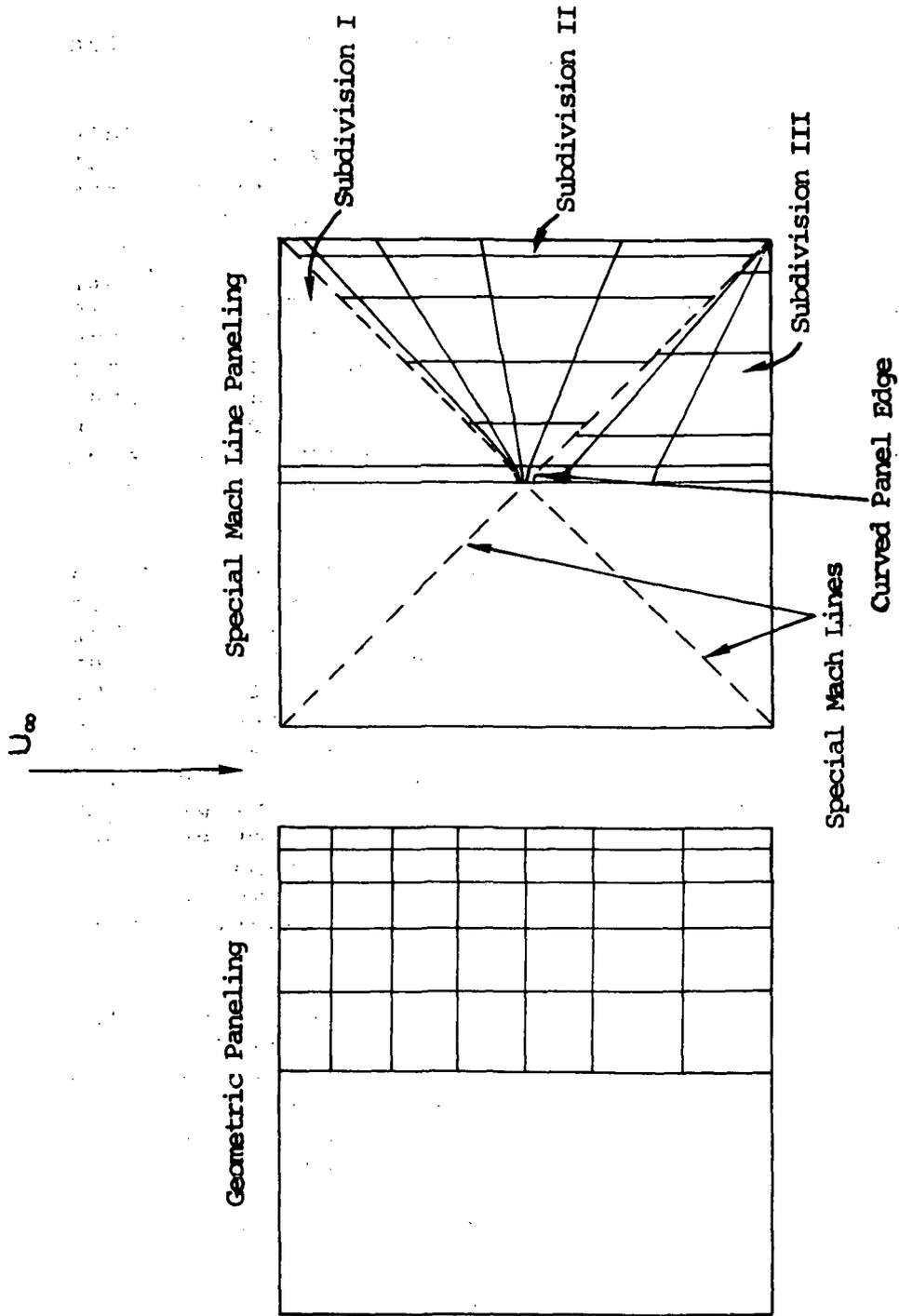
FIGURE 14 - SUPERSONIC PANELING SCHEMES

41

5.3 Evaluation of Kernel Function Integrals

Equation (11) gave the integral expression which relates the downwash, w, to the vorticity distribution, γ. Equations (12) and (13) gave the kernel functions appearing in the integral for subsonic and supersonic flow, respectively. This section discusses the evaluation of the integral for both flow regimes and the additional problem of establishing the limits for the supersonic integral.

Substituting the expression for γ_j, the basic spline distribution of vorticity (Equation (25)), into the downwash integral (Equation (11)) gives the downwash at point i due to unit amplitude of the jth spline distribution:

$$w_{ij} = \int_{y_L}^{y_R} \int_{x_{LE(\eta)}}^{x_{TE(\eta)}} \left[X(\zeta,\eta)Y(\eta) \right]_j K(\zeta-x_i, \eta-y_i)\,d\zeta\,d\eta \qquad (32)$$

where $[XY]_j$ denotes the right hand side of Equation (25). y_L and y_R are the left and right edges, respectively, of the panel associated with x_j y_j^m (components of $[XY]$). $X_{TE}(\eta)$ and $X_{LE}(\eta)$ are the trailing and leading edges, respectively, of that same panel. The symbol $\oint$ refers to the principle value of the integral (Ref. 5, pg. 132). The total downwash at x_i, y_i is then the sum of the influences from all the integrals for the various spline distributions, each multiplied by its respective strength, S_j. w_{ij} in Equation (32), corresponds to A_{ij} in Equation (16):

$$w_i = \sum_{j=1}^{N} A_{ij} S_j \qquad (16)$$

Examination of the integral in Equation (32) shows that since y_L and y_R are constants, due to the fact that they are parallel edges, the integration can best be performed on ζ first. Returning to Equations (26) and (27) for X, it is noted that both can be written as:

$$X = \pm \frac{\zeta - f(\eta)}{c(\eta)} \qquad (33)$$

where the variables of integration, ζ and η, replace x and y, respectively. Substituting Equation (33) into (32) and replacing A_{ij} for w_{ij} yields two general forms:

$$A_{ij}^1 = \pm \int_{y_L}^{y_R} Y(\eta) \frac{d\eta}{c(\eta)} \int_{x_{LE}(\eta)}^{x_{TE}(\eta)} \zeta K(\zeta - x_1, \eta - y_1) d\zeta \qquad (34)$$

and

$$A_{ij}^2 = \mp \int_{y_L}^{y_R} Y(\eta) \frac{f(\eta)}{c(\eta)} d\eta \int_{x_{LE}(\eta)}^{x_{TE}(\eta)} K(\zeta - x_1, \eta - y_1) d\zeta \qquad (35)$$

For arbitrary edges the integrations indicated by Equations (34) and (35) cannot be performed analytically for both ζ and η. The integration in the ζ direction can be performed analytically, however, leaving the integration in the η direction to be performed numerically. Even for the special cases when the integration can be performed entirely analytically (e.g., rectangular panels), it is faster to perform the outer, η integration numerically. This is because of the number of hyperbolic functions, etc. which arise from the analytical expression and must be evaluated by the computer.

Letting:

$$G_1(\eta) = \int_{x_{LE}(\eta)}^{x_{TE}(\eta)} \zeta K(\zeta - x_1, \eta - y_1) d\zeta \qquad (36)$$

and

$$G_2(\eta) = \int_{x_{LE}(\eta)}^{x_{TE}(\eta)} K(\zeta - x_1, \eta - y_1) d\zeta \qquad (37)$$

the resulting expressions for $G(\eta)$ in subsonic flow can be written as:

$$G_1(\eta) = \frac{1}{4\pi} \frac{\zeta}{(y_1 - \eta)^2} \left[\frac{\zeta^2}{2} - \frac{(x_1 + \zeta)}{2} \sqrt{(x_1 - \zeta)^2 + \beta^2(y_1 - \eta)^2} \right]$$

$$- \frac{\beta^2}{8\pi} \ln \left| (x_1 - \zeta) + \sqrt{(x_1 - \zeta)^2 + \beta^2(y_1 - \eta)^2} \right| \Bigg|_{\zeta = x_{LE}(\eta)}^{\zeta = x_{TE}(\eta)} \qquad (38)$$

$$G_2(\eta) = \frac{1}{4\pi} \frac{1}{(y_1 - \eta)^2} \left[\zeta - \sqrt{(x_1 - \zeta)^2 + \beta^2(y_1 - \eta)^2} \right] \Bigg|_{\zeta = x_{LE}(\eta)}^{\zeta = x_{TE}(\eta)} \qquad (39)$$

and in supersonic flow as:

$$G_1(\eta) = -\frac{1}{2\pi}\left[\frac{x_1 + \zeta}{2(y_1 - \eta)^2}\sqrt{(x_1-\zeta)^2 - \beta^2(y_1-\eta)^2}\right.$$
$$\left. + \frac{\beta^2}{2}\ln\left|(x_1-\zeta)+\sqrt{(x_1-\zeta)^2-\beta^2(y_1-\eta)^2}\right|\right]\begin{array}{l}\zeta = x_{TE}(\eta)\text{ or } x_{ML}(\eta)\\[12pt]\zeta = x_{LE}(\eta)\end{array}\qquad(40)$$

$$G_2(\eta) = -\frac{1}{2\pi}\frac{1}{(y_1-\eta)^2}\sqrt{(x_1-\zeta)^2-\beta^2(y_1-\eta)^2}\;\begin{array}{l}\zeta = x_{TE}(\eta)\text{ or } x_{ML}(\eta)\\[12pt]\zeta = x_{LE}(\eta)\end{array}\qquad(41)$$

The notation at the right side of the above expressions is the standard one for integrals, indicating that the expression is first evaluated with ζ replaced by the upper limit and then, subtracted from that, the expression with ζ replaced by the lower limit.

Under certain circumstances Equations (38) through (41) can become singular due to the $(y_1-\eta)^2$ term in the denominator. The order and presence of a singularity in the integrand depend on the relationship of y_1 to the two side edges of a panel, y_L and y_R, and the relationship of x_1 to the other two edges $x_{LE}(\eta)$ and $x_{TE}(\eta)$. It is obvious that if the control point y value falls to the left of y_L (the left edge) or to the right of y_R (the right edge) the integrals involving $(y_1-\eta)$ will never be singular. For this case, the numerical integration with respect to η from y_L to y_R can be performed routinely using Gaussian quadrature. It is also true, but less obvious, that if the x value of the control point, x_1, lies upstream of $x_{LE}(y_1)$ then there will be no singularity regardless of the y_1 value (this can be verified by taking the limit of the expression evaluated at both limits as η approaches y_1). For this last case, however, care must be taken that none of the quadrature points falls too close to y_1, when y_1 falls between y_L and y_R. Such proximity could give rise to numerical problems. Other than taking this precautionary measure, the integration is routine.

If the y_1 value falls between y_L and y_R and the x_1 value is downstream of the leading edge, $x_{LE}(y_1)$, then the $G(\eta)$ functions cannot be integrated directly. For this case there will be three basic singular forms: 1) a logarithmic singularity (for only the linearly varying terms, G_1), 2) a Cauchy singularity ($1/y_1-\eta$ form), and 3) a Mangler singularity ($1/(y_1-\eta)^2$ form). The first singularity is integrable in a Riemanian sense, but the latter two are not. These singular forms arise from taking the limiting form of the kernel function as the point of evaluation approaches the

44

plane of the singularity. There would be no singularities if the limiting process had been taken after the integration. The advantage of taking this limit before integrating is the resulting simpler expression. The cost of taking this limit is the introduction of the singular forms. Although the Mangler and Cauchy expressions cannot be numerically integrated, they can be eliminated from the integrand and treated separately (Ref. 7). There are several ways to accomplish this, but basically all the methods assume that the integrand can be expanded about the singularity as:

$$\overline{G}(\eta) = \frac{A_M}{(y_1-\eta)^2} + \frac{A_C}{(y_1-\eta)} + A_L \ln\left|(y_1-\eta)\right| + A_0 + A_1(y_1-\eta) + A_2(y_1-\eta)^2 + \cdots \quad (42)$$

Here $\overline{G}(\eta)$ represents either $G_1(\eta)$ or $G_2(\eta)$ multiplied by the remaining η functionality (from Equations (34) and (35)).

Expansion 42 can be performed either analytically or numerically. The analytical method is covered in Reference 7, so it will not be repeated here.

Numerically $\overline{G}(\eta)$ can be expressed as:

$$\overline{G}(\eta) = \overline{G}_S(\eta) + \overline{G}_R(\eta) \quad (43)$$

where $\overline{G}_S(\eta)$ contains all the singular forms and $\overline{G}_R(\eta)$ is regular. In the vicinity of the singularity, the leading terms of the series in Equation (42) dominate, therefore:

$$\overline{G}(\eta) \cong \frac{A_M}{(y_1-\eta)^2} + \frac{A_C}{y_1-\eta} + A_L \ln\left|y_1-\eta\right| + A_0 \quad (44)$$

(In region of singularity)

The only term of the above series which is antisymmetric about the singularity is the Cauchy term, $A_C/y_1-\eta$, therefore, it is possible to evaluate the coefficient of this term independently by computing $\overline{G}(\eta)$ at two points close to the singularity $\eta = y_1 + \epsilon_1$ and $\eta = y_1 - \epsilon_1$:

$$A_C \cong \frac{\epsilon_1}{2}\left[\overline{G}(y_1-\epsilon_1) - \overline{G}(y_1+\epsilon_1)\right] \quad (45)$$

The choice of ϵ_1 is a function of the number of significant figures the machine uses to store numbers and, to a lesser extent,

the manner in which the expression for $\overline{G}(\eta)$ is constructed. (The accuracy of $\overline{G}(\eta)$ near the singularity is best if the origin of the axis system is located at the singularity. This origin location avoids the numerical problem of adding a small number to a large one.)

Since the remaining terms of Equation (44) are all symmetric about the singularity, they must be evaluated simultaneously. The three unknowns A_M, A_L, and A_0 can be numerically computed by evaluating $\overline{G}(\eta)$ at three points. Because the Cauchy term has a rather large influence, numerical error can be reduced by eliminating this antisymmetric term (as well as the other antisymmetric terms) from the calculation by evaluating $\overline{G}(\eta)$ at equal distances on both sides of the singularity and summing the influences. This gives three equations for the three unknowns:

$$\frac{2}{\epsilon_1^2} A_M + 2\ln|\epsilon_1|A_L + 2A_0 = \overline{G}(y_1 + \epsilon_1) + \overline{G}(y_1 - \epsilon_1) \qquad (46a)$$

$$\frac{2}{\epsilon_2^2} A_M + 2\ln|\epsilon_2|A_L + 2A_0 = \overline{G}(y_1 + \epsilon_2) + \overline{G}(y_1 - \epsilon_2) \qquad (46b)$$

$$\frac{2}{\epsilon_3^2} A_M + 2\ln|\epsilon_3|A_L + 2A_0 = \overline{G}(y_1 + \epsilon_3) + \overline{G}(y_1 - \epsilon_3) \qquad (46c)$$

These equations can be solved for A_M and A_L. A_0 will not be required as will be shown next.

Using the above results, $\overline{G}_S(\eta)$, Equation (43), can be expressed as:

$$\overline{G}_S(\eta) = \frac{A_M}{(y_1 - \eta)^2} + \frac{A_c}{y_1 - \eta} + A_L \ln\left|y_1 - \eta\right| \qquad (47)$$

The above expression can be integrated directly using the integrals given for the Mangler and Cauchy forms in Reference 7.

$$\int_{y_L}^{y_R} \frac{A_M}{(y_1 - \eta)^2}\, d\eta \equiv A_M \left[\frac{1}{(y_1 - y_R)} - \frac{1}{(y_1 - y_L)}\right] \qquad (48)$$

46

$$\int_{y_L}^{y_R} \frac{A_C}{y - \eta} \, d\eta \equiv A_C \left[-\ln \left| \frac{y_1 - y_R}{y_1 - y_L} \right| \right] \tag{49}$$

$$\int_{y_L}^{y_R} A_L \ln |y_1 - \eta| \, d\eta = A_L \left[-(y_1 - y_R) \ln |y_1 - y_R| \right.$$
$$\left. + (y_1 - y_L) \ln |y_1 - y_L| - y_R + y_L \right] \tag{50}$$

The non-singular part of $\overline{G}(\eta)$ is then:

$$\overline{G}_R(\eta) = \overline{G}(\eta) - \overline{G}_S(\eta) = \overline{G}(\eta) - \frac{A_M}{(y_1 - \eta)^2} - \frac{A_C}{y_1 - \eta} - A_L \ln |y_1 - \eta| \tag{51}$$

The above expression picks up the A_0 and remaining terms which were dropped to compute the A_M, A_C, and A_L. $\overline{G}_R(\eta)$ contains no forms which cannot be integrated numerically using Gaussian quadrature. Therefore, numerical integration of $\overline{G}_R(\eta)$, when combined with the results shown in Equations (48) through (50), constitute the entire integration of $\overline{G}(\eta)$ to evaluate A_{ij}. (It is important to mention again that the allowable magnitudes for ϵ_1, ϵ_2, and ϵ_3 depend on the number of significant figures carried for $G(\eta)$ and are therefore computing machine dependent.)

The above procedure was compared to a method which used the non-singular, out of plane expression for the kernel. This alternate procedure integrates the out of plane kernel using a control point very close to the singularity plane. For the same accuracy, the planar computational scheme, just described, was about ten times faster. Both schemes used a self checking integrator which breaks the interval of integration into parts small enough to be handled by a four point Gaussian quadrature using eight points as a check (Reference 8).

The ζ integration in supersonic flow is not always between the leading and trailing edges. Figure 15 shows the forward Mach lines emanating from the point x_1, y_1. These lines are shown cutting a panel, the significance of this cut is that portions of the panel ahead of the lines influence the point x_1, y_1, while those aft do not. In terms of the kernel function, the regions aft of the lines cause the values in the radicals to become negative making the expression for the integrand complex. Physically, this means that the influencing region is limited to the area within the forward Mach lines, therefore, the limits of integration should be adjusted to include only this region. Figure 15 shows two distinct regions of integration, one from the panel leading edges to the panel trailing edges - Region I; and one from the panel leading edges to the Mach lines - Region II. The integration over a panel is the sum of the integrals over the
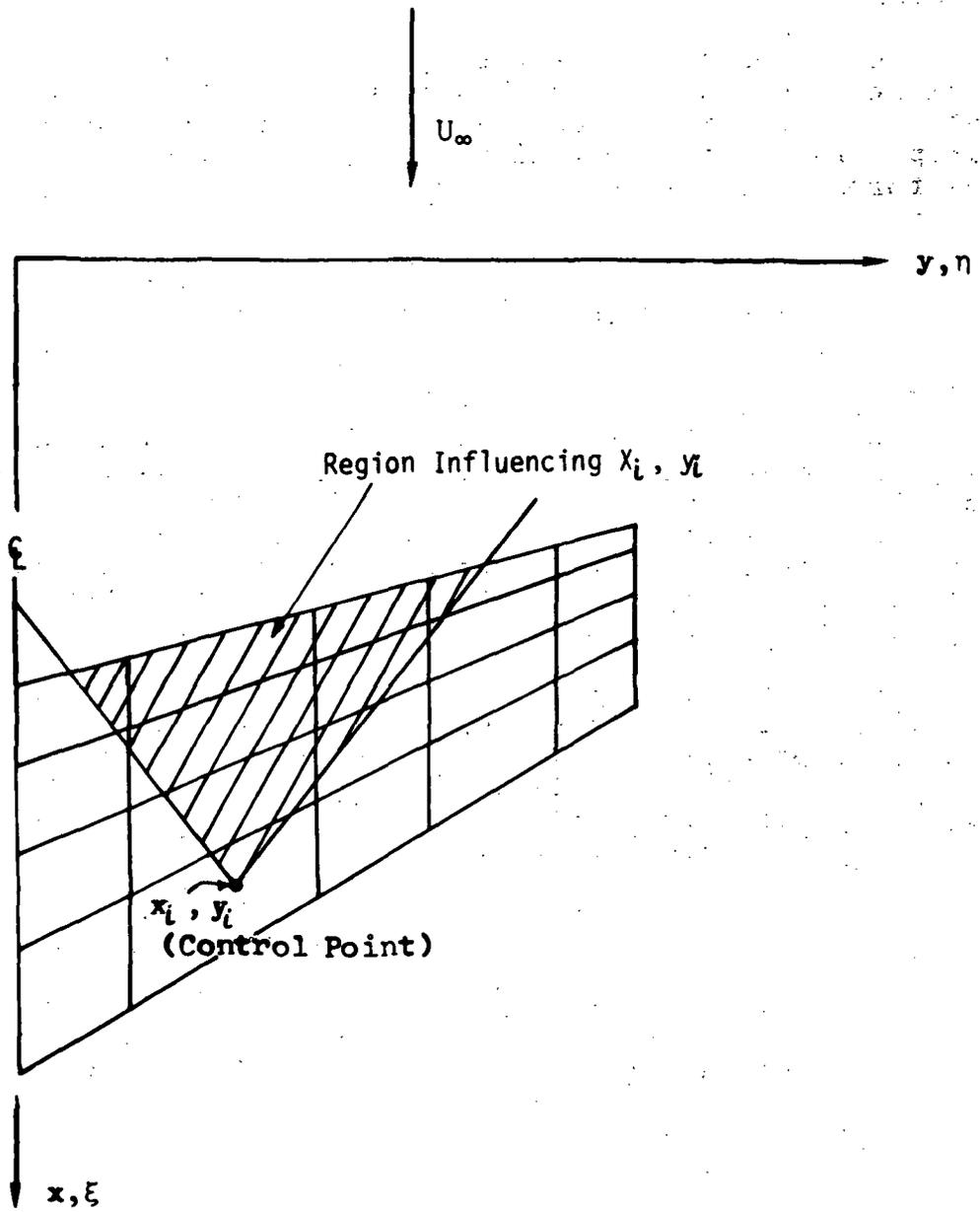
FIGURE 15 - FORWARD MACH CONE ON SURFACE OF A WING

two types of regions (as will be shown in Figure 16, there can be several of each type on a single panel).

The integration of the supersonic kernel in the ζ direction from leading edge to trailing edge was given in Equations (40) and (41). The integral from leading edge to Mach line is the same except for the upper limit, $X_{TE}(\eta)$, replaced by the equation of the forward Mach line:

$$\zeta_{ML} = x_1 \mp \beta(\eta - y_1) \qquad \begin{array}{l} - \text{ right going Mach line} \\ \\ + \text{ left going Mach line} \end{array} \qquad (52)$$

This upper limit on ζ simplifies the expressions in Equations (40) and (41) by forcing the radicals to vanish. The integrands for the η integration which result from this changing of limits on ζ are therefore no more complicated to integrate than the ones already discussed. The problem then is identifying the various regions on the panel so that the limits for the η integrations can be determined.

For curved panel edges, a Mach line can intersect in various ways. Figure 16 shows some of these combinations. Several intersection characteristics can be noted from the figure:

1. After an intersection with a trailing edge, the Mach line can intersect either the trailing edge again or the leading edge.

2. After an intersection with a leading edge the Mach line can intersect either the leading edge again or the trailing edge.

3. Proceeding left to right (positive η or y direction) each intersection changes the region - from a Region I to a Region II from a Region II to a Region I and from a Region II to a Region 0 (Region 0 does not influence the control point); but there can never be a jump from a Region I to a Region 0 or vice versa.

The above characteristics can be used to form a logical scheme to identify the various regions and find the limits of integration. Using the quadratic equation for the planform edges from Figure 13 and the equation for the Mach lines (52) expressed in a common coordinate system, a quadratic expression for the intersections can be obtained:

$$x_1 \mp \beta(\eta - y_1) - a - b\eta - c\eta^2 = 0 \qquad (53)$$

where $a + b\eta + c\eta^2$ is the equation of the panel edge .

y,n

y_R y_L

U_∞

Region II

x,n

Side - Side

Leading edge - trailing edge

Trailing edge - trailing edge

Panel

Region I

None

Region 0

None (No influence)

Trailing edge - leading edge

Side - Leading Edge

Trailing edge - side

Side - Leading edge - leading edge - side

Side - leading edge - leading edge - trailing edge

Side - leading edge - leading edge - trailing edge

Region 0   No integration

Region I   Integration leading edge to trailing edge

Region II   Integration leading to Mach line

FIGURE 16 - TYPICAL FORWARD MACH LINE INTERSECTIONS WITH A PANEL

50

The four roots of this expression (two for the $+\beta$ and two for the $-\beta$) represent the four possible intersections of the panel leading or trailing edges and their extensions with the Mach line. A total of eight roots are obtained when both leading and trailing edges are considered. The scheme to identify the regions and limits on η takes these eight roots and arranges them so that they are in order according to their η value (from left to right). With each root is an identifier which states whether the root belongs to the leading or trailing edge. Roots to the left of the left panel edge (y_L) are excluded as well as roots to the right of the right panel edge (y_R).

The integration limit determination procedure starts by establishing whether the Mach line crosses the left panel edge ahead, behind, or on the panel. If ahead of the panel, the first region, bounded by y_L and the first intersection (which has to be with the leading edge) will be a Region 0 (no integration - no influence). If on the panel, the first region will be a Region II. If behind the panel, the first region will be a Region I. If there are no intersections (roots) between y_L and y_R then the entire panel is of the same region type. The key region is Region II. From this region, the next region will be either 0 or I depending whether the intersection is with the leading or trailing edge respectively. In going from one region to another, Region II will always be involved.

Figure 17 shows the logic block used to establish the limits. Once the procedure is started, at the left panel edge, it proceeds automatically with y_L being the first limit and y_R being the last. As an example of how the logic block results are used, Figure 17 also shows the regions and η limits of integration for a right going Mach line whose origin is positioned behind the left panel edge (R_i denotes a root of Equation (53)).

One quick test which can be made to see if a panel has any influence on a control point before using the above logic is to check the x_i value versus the most forward ζ value of the panel edge. If x_i is upstream of this ζ value then the panel cannot influence the control point regardless of the supersonic Mach number. This computation can save evaluating the sorting roots in many instances.

Because the supersonic flow problem requires this added computation, which involves only the panel-control point relationship, and since each panel is covered by several Y_j, it is advantageous to integrate all the possible components of each spline function which share a particular panel-control point relationship. That is, the contributions to A_{ij} from each of the twelve components of Y_j in (Equation (25)) are not summed consecutively, but rather are added to as the program loops from

$$\int_{y_L}^{y_R} G(\eta)\bigg|_{x_{LE}}^{x_{TE} \text{ or } x_{ML}} d\eta = \underbrace{\int_{y_L}^{R_1} G(\eta)\bigg|_{x_{LE}}^{x_{TE}} d\eta}_{\text{Region I}} + \underbrace{\int_{R_1}^{R_2} G(\eta)\bigg|_{x_{LE}}^{x_{ML}} d\eta}_{\text{Region II}} + \underbrace{\int_{R_2}^{y_R} (0) d\eta}_{\text{Region 0}}$$

FIGURE 17 - LOGIC BLOCK TO SET LIMITS OF SUPERSONIC INTEGRALS

52

one panel to another. This means that the total value of A_{ij} may not be available until all integrations over all the panels have been performed. Such an arrangement avoids setting the region limits more than once for any control point-panel relationship. This procedure offers a computational speed advantage over another possible arrangement which forms one complete A_{ij} before going to the next (i.e., a complete γ_j). With this latter arrangement, the region limits must be computed several times for the same control-point panel relationship, due to the spline arrangement where functions occupy common panels (Figures 10 and 12).

This concludes the basic formulation of the numerical integration scheme used to evaluate A_{ij} (termed the influence coefficient elements). The next section describes how these elements are used to match the boundary conditions for various flow problems.

5.4 Satisfaction of Boundary Conditions on Singularity Surfaces

The preceeding sections showed the construction of the basic building block of the numerical scheme - the vortex spline. This section shows how the strengths, S_j (multiplicative constants of each γ_j), are determined by application of the boundary conditions on the singularity surface (region "s" of Equation (11)). Each element naturally satisfies the governing differential equation, since they were developed from the horseshoe vortex, and each element also satisfies all the continuity of vorticity required of the final solution (the purpose of the spline), therefore the strengths of these elements are all independent. This independency means that every element can be separately adjusted such that it best satisfies the imposed boundary conditions. Since the splines have a limited number of degrees of freedom, they, in general, cannot exactly satisfy these boundary conditions. A compromise match must be accepted. The compromise used for the spline development was a least square error match. A solution based on this technique will yield the best overall fit to the boundary conditions.

The square error involved in the approximation to the boundary conditions can be mathematically expressed as:

$$E^2 = \int\int_{s} \left[W_{BC}(\zeta,\eta) - W_S(\zeta,\eta) \right]^2 d\zeta \, d\eta \qquad (54)$$

where E^2 is the square error, $W_{BC}(\zeta,\eta)$ is the applied downwash boundary condition and $W_S(\zeta,\eta)$ is the downwash from the splines. Since it is not possible to perform the indicated surface integration for general cases, an approximation has to be made. This is done by assuming the integral can be expressed as a weighted sum:

$$E^2 \cong \sum_{l=1}^{M} \left[W_{BC}(\zeta_l,\eta_l) - W_S(\zeta_l,\eta_l) \right]^2 a_l \qquad (55)$$

Here (ζ_l, η_l) is one of M points on the surface (termed the control points) and a_l is an area associated with that point. (The choice of control point locations and their associated areas is discussed later.) Equation (16) can be used to express $W_S(\zeta_l,\eta_l)$ in Equation (55) giving:

$$E^2 \cong \sum_{l=1}^{M} \left[W_{BC_l} - \sum_{j=1}^{N} A_{lj} S_j \right]^2 a_l \qquad (56)$$

54

The notation has been abreviated such that the subscript i denotes the value at (ζ_i, η_i).

The square error in Equation (56) can be minimized with respect to each strength, S_j, since these strengths are independent. This minimization is accomplished by differentiating Equation (56) with respect to S_k and setting the resulting expression to zero:

$$\frac{\partial E^2}{\partial S_k} = 2 \sum_{i=1}^{M} \left[W_{BC_i} - \sum_{j=1}^{N} A_{ij} S_j \right] a_i A_{ik} = 0 \qquad (57)$$

The variable, k, ranges from 1 to N, therefore Equation (57) represents N algebraic equations which can be solved for the N strengths. A more useable form for Equation (57) is:

$$\sum_{i=1}^{M} \sum_{j=1}^{N} A_{ik} a_i A_{ij} S_j = \sum_{i=1}^{M} A_{ik} a_i W_{BC_i} \qquad (58)$$

The entire set of Equations (58) can be written in matrix notation as:

$$\underset{\substack{NxM}}{\left[A \right]^T} \underset{\substack{MxM}}{\left\lceil a \right\rfloor} \underset{\substack{MxN}}{\left[A \right]} \underset{\substack{Nx1}}{\left\{ S \right\}} = \underset{\substack{NxM}}{\left[A \right]^T} \underset{\substack{MxM}}{\left\lceil a \right\rfloor} \underset{\substack{Mx1}}{\left\{ W_{BC} \right\}} \qquad (59)$$

Here $\left[A \right]^T$ is the transpose of matrix $\left[A \right]$ with elements A_{ij}, and $\left\lceil a \right\rfloor$ is a diagonal matrix with elements a_i. The $\left\{ S \right\}$ and $\left\{ W_{BC} \right\}$ are vectors representing the unknown strengths, and the known boundary conditions, W_{BC_i}. Solving Equation (59) for $\{S\}$ gives:

$$\left\{ S \right\} = \left[\left[A \right]^T \left\lceil a \right\rfloor \left[A \right] \right]^{-1} \left[A \right]^T \left\lceil a \right\rfloor \left\{ W_{BC} \right\} \qquad (60a)$$

Equation (60a) is valid whenever the number of control points is greater than or equal to the number of unknowns ($M \geq N$). If the number of control points is equal to the number of unknowns ($M = N$) then [A] is a square matrix and Equation (60a) reduces to the determinate form of:

$$\left\{ S \right\} = \left[A \right]^{-1} \left\{ W_{BC} \right\} \qquad (60b)$$

An abreviated notation is introduced here:

$$\tilde{A}^T \equiv [A]^T \lceil a \rfloor \tag{61a}$$

$$A = [A] \tag{61b}$$

$$S = \{S\} \tag{61c}$$

$$W_{BC} = \{W_{BC}\} \tag{61d}$$

then

$$S = (\tilde{A}^T A)^{-1} \tilde{A}^T W_{BC} \tag{62}$$

The symbol $\tilde{A}^T$ is the transpose of A weighted by $\lceil a \rfloor$.

When the special Mach line paneling is employed, the hyperbolic nature of the flow can be used to advantage by treating each region as a separate wing and solving the problem in steps. Figure 18 shows the arrangement of the panels with the associated [A] matrix partitioned into elements which represent the influence of subdivisions on themselves, A ; and elements which represent the influence of subdivisions on other subdivisions, B. It is obvious from this figure that it is very inefficient to solve this problem with this one large matrix. Instead, the problem can be divided into three separate, smaller problems, corresponding to the three subdivisions (I, II, III). If this is done, the three equations to be solved in a manner analogous to Equation (59) are:

$$A_I S_I = W_I \tag{63a}$$

56

FIGURE 18 - PARTITIONING OF AIC MATRIX FOR MACH LINE PANELING

57

$$A_{II} \, S_{II} = W_{II} - W_{II}' \qquad\qquad (63b)$$

$$A_{III} \, S_{III} = W_{III} - W_{III}' \qquad\qquad (63c)$$

where $\qquad\qquad\qquad\qquad\qquad\qquad\qquad\qquad\qquad$ (63d)

$$W_{II}' = B_{II,I} \, S_I$$

$$\qquad\qquad\qquad\qquad\qquad\qquad\qquad (63e)$$

$$W_{III}' = B_{III,I} \, S_I + B_{III,II} \, S_{II}$$

The subscripts denote the subdivisions and the quantities W_I, W_{II}, and W_{III} are the known downwashes in each subdivision. The right hand sides of Equation (63b) and (63c) can be thought of as "effective" downwashes for the independently treated downstream subdivisions.

Another computational consideration is the cost of performing the operations indicated in Equation (60). A more direct method can be employed if Equation (56) is rewritten as:

$$E^2 = \sum_{i=1}^{M} \left[W_{BC_i} \sqrt{a_i} - \sum_{j=1}^{N} \sqrt{a_i} \, A_{ij} S_j \right]^2 \qquad (64)$$

The above expression can be minimized directly using Householder's technique (Ref. 9). This procedure provides a great savings in computation time over the method represented by Equation (60).

The key feature of this least square error approach is to select the points (ζ_i, η_i) and the areas, a_i, such that Equation (55) does approximate Equation (54). With this goal, a study of various arrangements was undertaken. Fundamentally the study entailed subdividing the panels, which were used to form the splines. These subdivisions were formed by lines of constant percentage span and chord. Control points were located on these subdivisions using the area of the subdivision as the weighting factor, a_i, in Equation (55). These points were located at the spanwise centroids of the subdivisions, midway between the leading and trailing edges. In the study the number of spanwise sections could be specified independently from the chordwise sections.

Figure 19 shows the minimum arrangements resulting from the study for supersonic and subsonic flow. By minimum, it is meant that the arrangement's approximation to the integral (Equation (54)) was adequate over a wide variation of paneling. (Results presented later will show the accuracy of the arrangements for cases with as few as twelve panels and twenty-four control points.) The supersonic case required more control points because of the limited extent of influence in supersonic flow; consequently more points are needed to "sense" this influence.

The study also revealed that difficulties are encountered in the vicinity of subsonic leading edges and at all tips due to the singular nature of the vorticity distribution in these regions. Since the splines do not have the proper asymptotic form, the downwash has an improper singular behavior. This downwash departure tends to have a strong influence on the error minimization procedure if control points come too close to the edges involved. So, another study was made to determine suitable locations for control points in these regions. A review of other lifting surface schemes showed that their respective two-dimensional formulations could give the proper lift on a flat plate at angle of attack in subsonic flow using only one element (e.g., $N=1$ in Equation (16)). In fact, this is a criterion that can be used to establish the proper control point location for a determinate numerical formulation (where the number of unknown strengths is equal to the number of control points). This two dimensional criterion can be shown to be valid for the vortex lattice (Ref. 10) and the constant pressure panel schemes. Using this criterion, the proper control point location for the spline was computed. The one element spline representation for the lift on a flat plate is shown in Figure 20. The integrated load for the spline was set equal to the linear theory integrated load. The location was then found where the downwash from the spline is equal to the downwash on the flat plate. This location is at the center of the panel. (This result can be confirmed using Equation (18) with the distribution $\gamma(\zeta) = (x_2 - \zeta)/(x_2 - x_1)$). Starting with this result, it was discovered, by numerical investigation, that points on or downstream of the center chord line of the leading edge panel consistently produced accurate results. Since the components of the spanwise functions begin and end at the mid panel span, (Figure 10), the criterion in this direction is that the control points near an edge be on or inboard of the three quarter panel span (corresponding to the center of the half panel).

Using the above criteria, the general paneling arrangements shown in Figure 8 could be applied directly without any special considerations for subsonic flow, since the control point configuration satisfies the conditions outlined. For supersonic flow, there is no problem spanwise; chordwise, with a supersonic
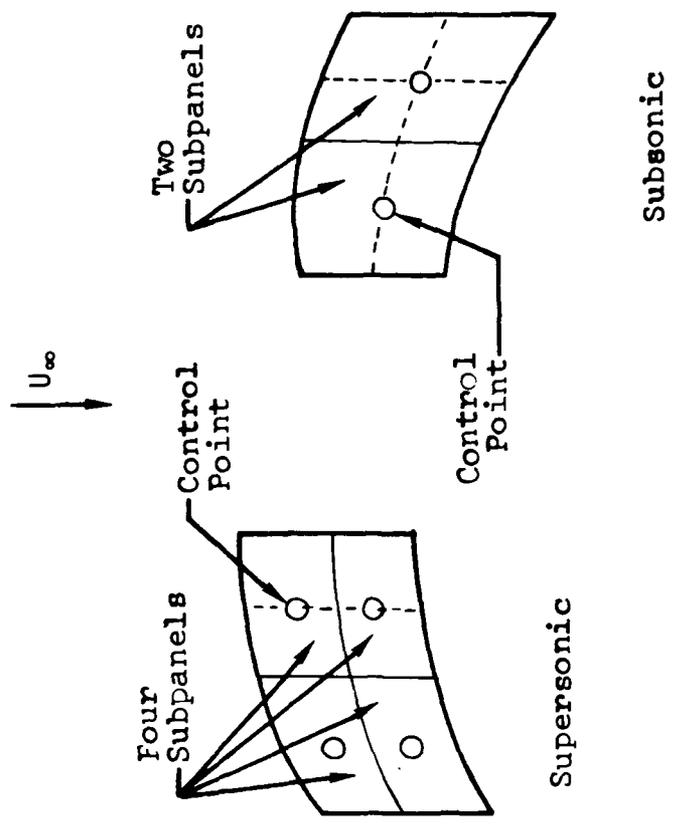
FIGURE 19 – CONTROL POINT CONFIGURATIONS ON A SINGLE PANEL
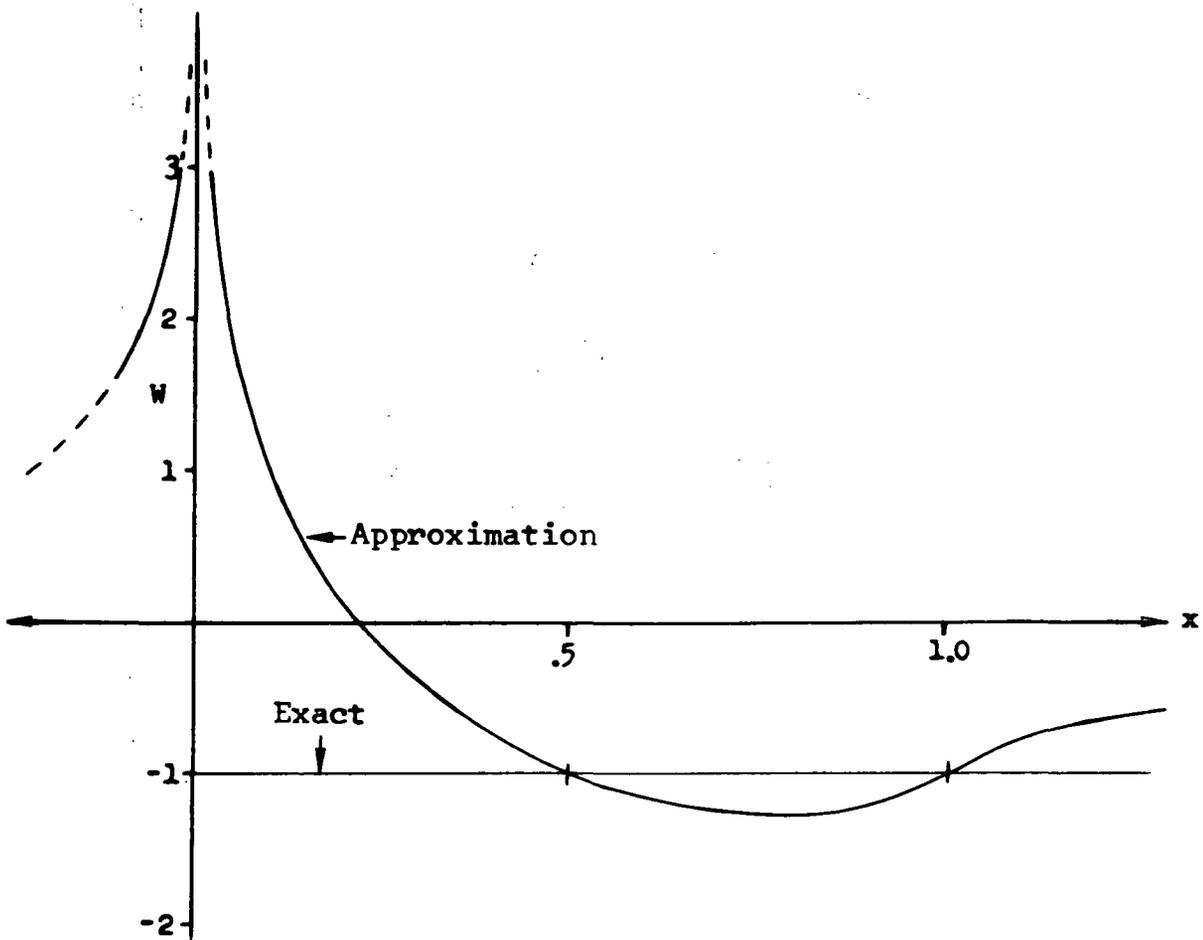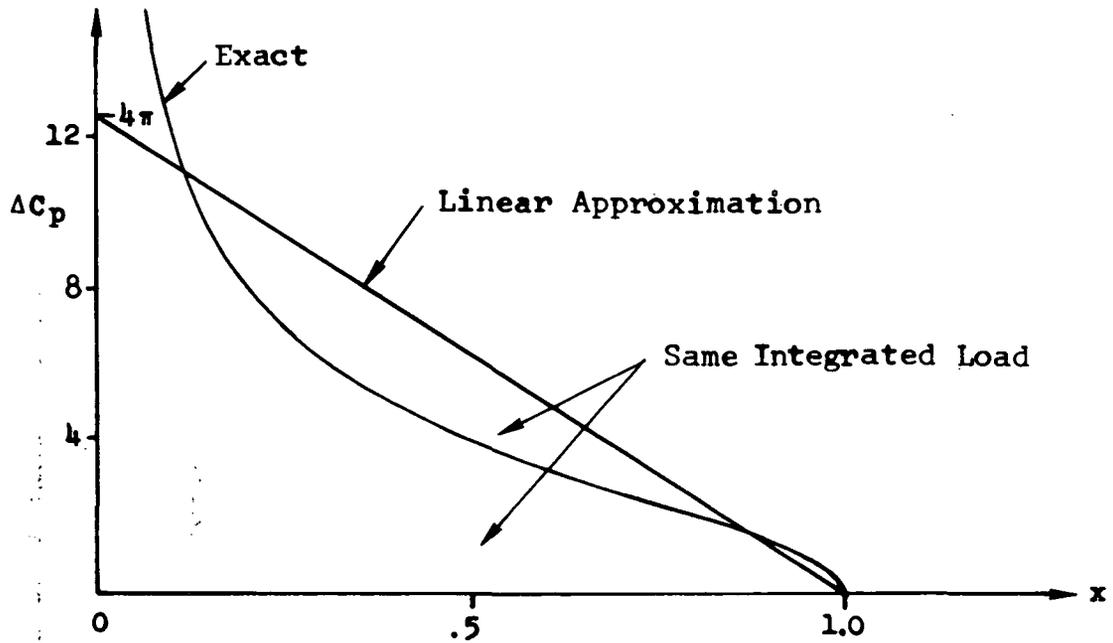
FIGURE 20 - TRIANGULAR PRESSURE DISTRIBUTION MODEL OF A FLAT
PLATE AT ANGLE OF ATTACK

61

leading edge, there is also no problem. But, if the leading edge is subsonic, the two forward control points must be excluded from the minimization process. With this simple exclusion rule, consistently accurate results were obtained over a wide range of test cases.

The benefit of this least square error scheme can be more fully realized for cambered surfaces where the number of functions needed to model a problem can be small compared to other schemes. This is because relatively few functions can model rather rapid camber variations and the number of functions is not tied one to one to the number of control points. With the least square error formulation, any number of control points per panel can be introduced to accurately incorporate the camber variation into the problem and at the same time, the number of functions can be held to a minimum. As pointed out earlier, the configurations shown in Figure 19 represented the minimum arrangement for consistent accuracy, any larger number of control points could also be used to obtain better camber definition, (subject to the edge constraints outlined above).

5.5 Computational Procedure

Figure 21 shows a flow diagram of a method to compute results using the vortex spline scheme. Once the strengths, S, have been computed, the remaining parameters can be determined (e.g., lift, moment, pressure distribution, etc.). Since the splines provide a continuous distribution over the surface, the pressure and bound vorticity can be evaluated directly at any point by determining the aggregate influence of the contributing functions. This continuity also makes it possible to compute the shed vorticity, σ, by integrating and differentiating the basic distribution for γ as indicated by Equation (23).

The lift and load distribution can be computed either by actually integrating the basic functions or by performing a sum on the pressures, similar to what was done for the least square downwash error integral formulation using the same control points and areas. The moment can likewise be computed by integrating or summing; however, the accuracy of this calculation using the summing technique is less than that for the lift calculation. Nevertheless, the summing technique is sufficiently accurate when several panels are employed and was the method used to compute both the lifts and moments presented in the next section.

In addition to the standard aerodynamic parameters, the mean square error can also be computed. This mean is the parameter, E_i^2 in Equation (55) divided by the total area (sum of the a_i). The mean square error (with appropriate control point exclusion) is an excellent indicator of the overall accuracy of the solution. The square root of this value, the root mean square downwash error, was found to be the same order of magnitude as the root mean square pressure error for the cases examined. This RMS error parameter supplies the user with an a posterior judgment of the validity of a flow model without the need to consult other data. It also opens the possibility of formulating a scheme which would automatically adjust the paneling and rerun a case if sufficient accuracy were not obtained from the initial run.

The next section presents the test cases that were used to evaluate the scheme.

Geometry

o Areas
o Control Point Locations
o Panel Descriptions

AIC Matrix
Generator

Solution Continues
for Additional Regions

o A & B

Downwash at Each Control Point Due to Each Function
(A - Aerodynamic Influence Coefficient Matrix)*

Least Square
Error AIC Matrix
Formulator

o $\tilde{A}^T A$

Least Square
Error Downwash
Matrix

"Effective"
Downwashes Used
For Downstream
Regions in Super-
sonic Flow
(See eqn.'s 63 b
and c)

o $\tilde{A}^T \{W\}$

Solution-
Strengths of
Singularities

o $\{S\} = \left[\tilde{A}^T A\right]^{-1} \tilde{A}^T \{W\}$ (eqn. 62)

o $\{W\} = B\{S\}$
(eqn.'s 63 d
and e)

Downwash at Points
in Downstream Regions

Bound Vorticity $\{\gamma\}$
Calculations

o Total C_L, C_M & Wing Bending Moment; Momt. & Load Dist
EXIT (After Additional Points)

Yes

Additional
Regions?

no

Error Analysis

o Errors Between Solution and True Downwashes

Yes

Additional points
at which the vorticity is desired

no

Exit

Mach Line Paneling Loop

* The influence of the functions on points outside the region of investigation
(Matrix B) are also computed. These points are used in the supersonic case to
compute the influence of one region (upstream) on another (downstream). This
technique allows the solution to be obtained by marching downstream.(see fig.18.)

o = Computed Quantity

(~) Denotes Weighted Matrix

FIGURE 21 - CONCEPTUAL FLOWCHART (FIRST ORDER)

5.6 Numerical Results

Various configurations were analyzed to determine paneling requirements and convergence to a known answer. The spline function results were compared with other lifting surface schemes and exact,linearized flow solutions. Figures 22 through 28 show the results.

Figure 22 is a comparison of the spline scheme with another lifting surface solution (Ref. 10) for a circular wing in incompressible flow. The comparison shows good agreement not only for the coefficients but also for the detailed loading. Note how well the quadratic edged panels can match the exact planform.

Figures 23 and 24 show comparisons of the spline scheme with a pressure mode scheme (Ref. 2) for compressible, subsonic flow. Again agreement is very good. Note the rounding of the planform representation at the root for both cases. This eliminated downwash singularities without introducing any special singular forms for γ .

Figure 25 shows a comparison of the spline scheme, using special Mach line paneling, with the exact, conical flow result (Ref. 11). The planform paneling shows a rounding at the root. This rounding produced a slight departure of the pressure from the exact result in the vicinity of the rounding (not noticeable in the chordwise plot of the pressure).

Figure 26 shows two comparisons of the spline scheme using geometric paneling for supersonic flow: one with the exact solution and one with a constant pressure panel scheme using the same paneling. Even for this paneling, which ignores the special Mach lines, the spline scheme gives accurate coefficient results with a reasonable comparison to the pressure.

Figure 27 shows another comparison of the spline scheme with exact conical flow results (Ref. 11). This planform has a subsonic leading edge. Again note the rounding of the planform. This rounding causes a local departure of the pressure from the exact result as shown. The overall agreement is good, even for the relatively few panels used.

Figure 28 shows the numerical stability of the formulation for various paneling schemes. In all cases the pressure distributions appear to be as accurate as could be expected for a

α = 1 RADIAN
M = 0

- - - - (REF 10)
——— VORTEX SPLINE

ΔC_p

10
5
0

ΔC_p

10
5
0

ΔC_p

10
5
0

U_∞

y

x

(N_0 is the neutral point expressed in terms of fraction mean chord aft of root chord leading edge.)

EXACT $\begin{cases} C_L = 1.790 \\ N_0 = 0.306 \end{cases}$

VORTEX SPLINE $\begin{cases} C_L = 1.782 \\ N_0 = 0.309 \end{cases}$
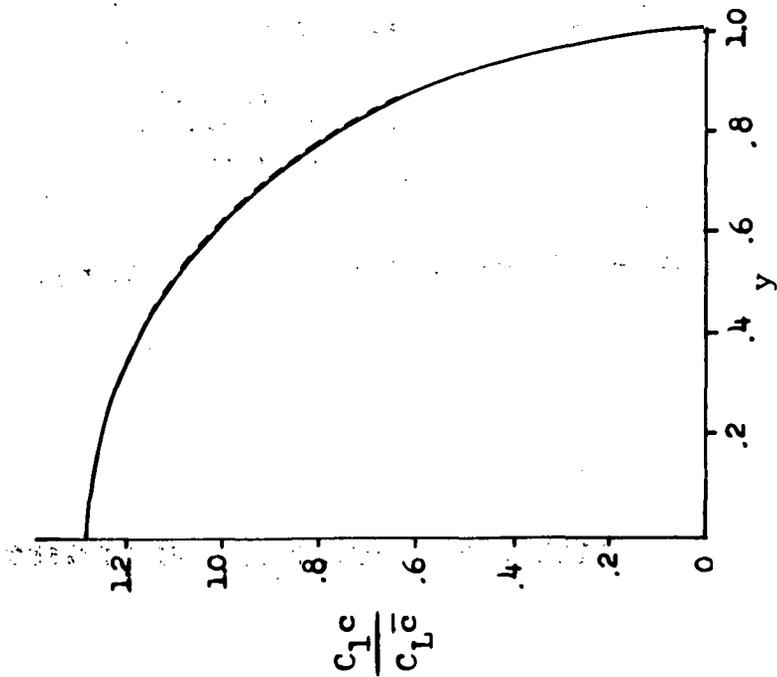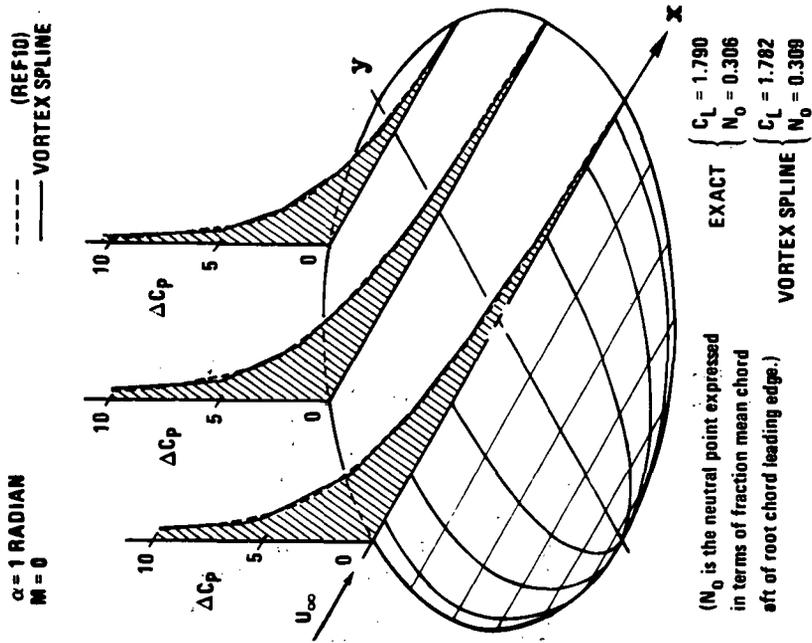
Root Mean Square Downwash Error = 4.85 $\times 10^{-2}$

$\dfrac{c_l c}{C_L \bar{c}}$

1.2
1.0
.8
.6
.4
.2
0

.2   .4   .6   .8   1.0
y

Spanwise Loading

FIGURE 22 – CIRCULAR WING
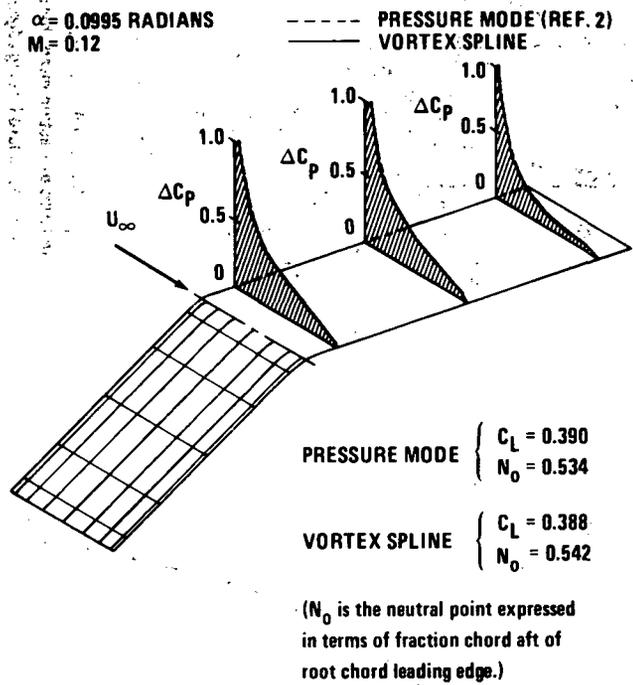
FIGURE 23 - UNTAPERED SWEPT WING
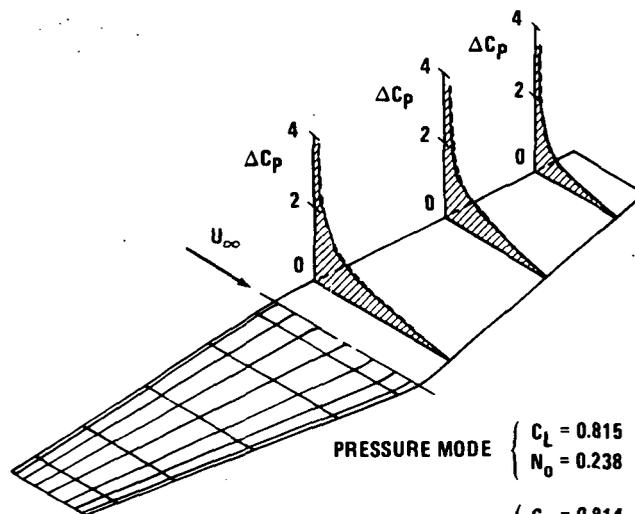
α = 0.199 RADIANS   – – – – PRESSURE MODE (REF. 2)
M = 0.15   ──── VORTEX SPLINE

ΔC_P

U_∞

PRESSURE MODE $\begin{cases} C_L = 0.815 \\ N_0 = 0.238 \end{cases}$

VORTEX SPLINE $\begin{cases} C_L = 0.814 \\ N_0 = 0.244 \end{cases}$

(N_0 is the neutral point and is
expressed in terms of fraction mean
chord aft of root chord leading edge.)

Root Mean Square Downwash Error   = 1.81×10^{-2}

FIGURE 24 – TAPERED WING WITH ZERO SWEEP OF QUARTER CHORD
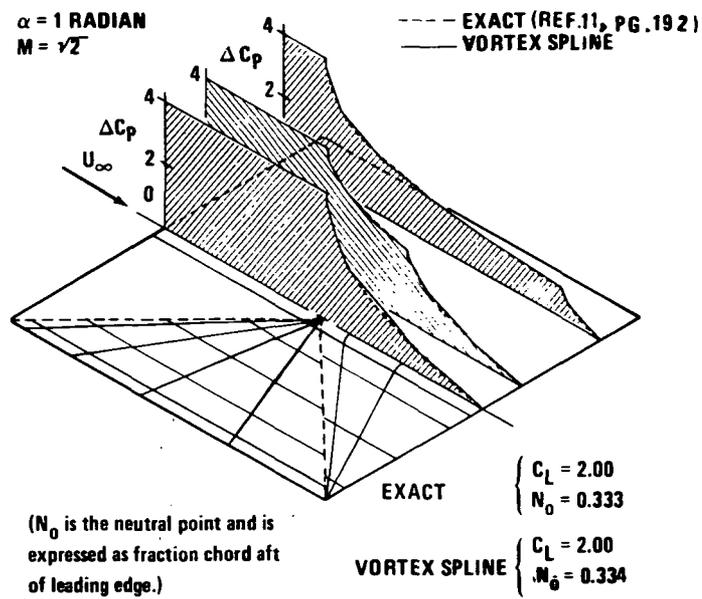
FIGURE 25 - SQUARE WING (SPECIAL MACH LINE PANELING)

$\alpha = $ 1 RADIAN
$M = \sqrt{2}$

- - - - - EXACT (REF.11, PG.192)
——— VORTEX SPLINE
⌐L CONSTANT PRESSURE PANELS

ΔC_P

ΔC_P

U_∞

EXACT $\begin{cases} C_L = 2.00 \\ N_0 = 0.333 \end{cases}$
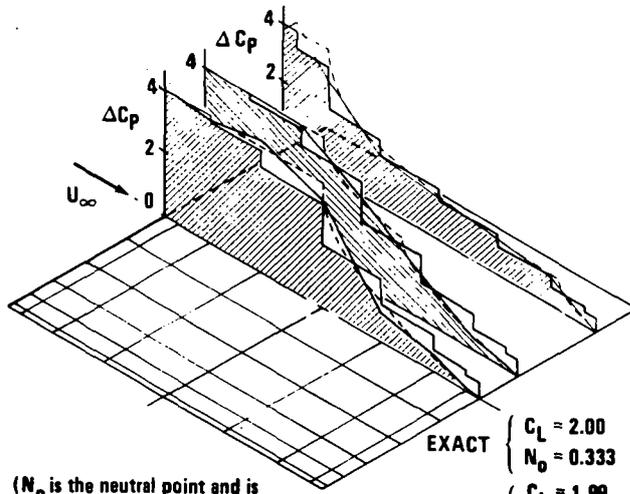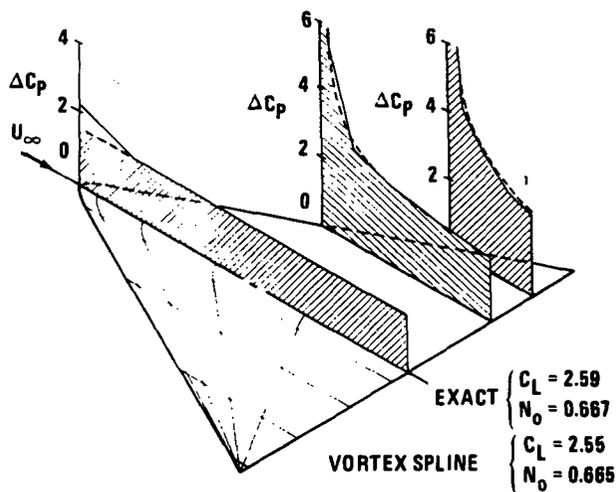
(N$_0$ is the neutral point and is expressed as fraction chord aft of leading edge.)

VORTEX SPLINE $\begin{cases} C_L = 1.99 \\ N_0 = 0.334 \end{cases}$

CONSTANT PRESSURE PANELS $\begin{cases} C_L = 2.07 \\ N_0 = 0.357 \end{cases}$

Root Mean Square Downwash Error $= 1.79 \times 10^{-2}$

FIGURE 26 - SQUARE WING (GEOMETRIC PANELING)

FIGURE 27 - DELTA WING

α = 1 RADIAN
M = 0
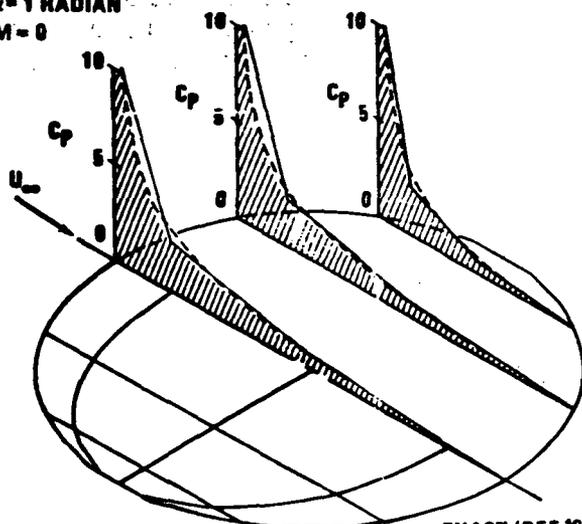
(N$_0$ is the neutral point expressed in terms of fraction mean chord aft of root chord leading edge.)

---- EXACT (REF.10)
—— VORTEX SPLINE

EXACT $\begin{cases} C_L = 1.790 \\ N_0 = 0.306 \end{cases}$

a. VORTEX SPLINE $\begin{cases} C_L = 1.793 \\ N_0 = 0.330 \end{cases}$

Root Mean Square Downwash Error = 9.65×10^{-2}

b. VORTEX SPLINE $\begin{array}{l} C_L = 1.784 \\ N_0 = 0.320 \end{array}$
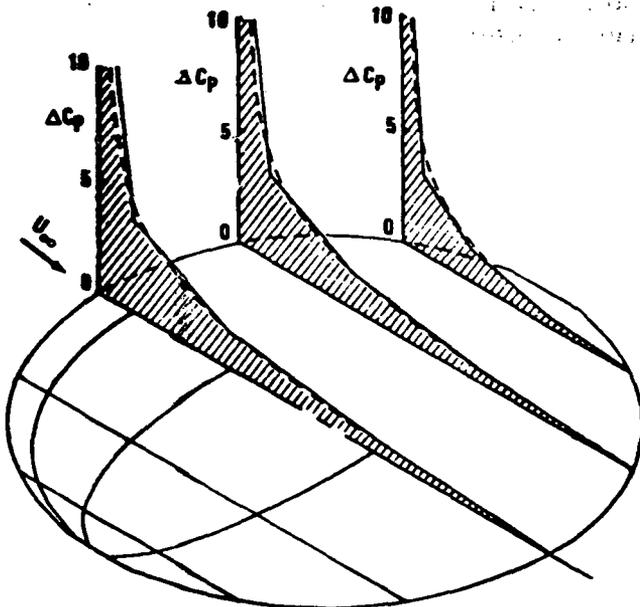
Root Mean Square Downwash Error = 1.02×10^{-1}

c. VORTEX SPLINE $\begin{cases} C_L = 1.794 \\ N_0 = 0.321 \end{cases}$
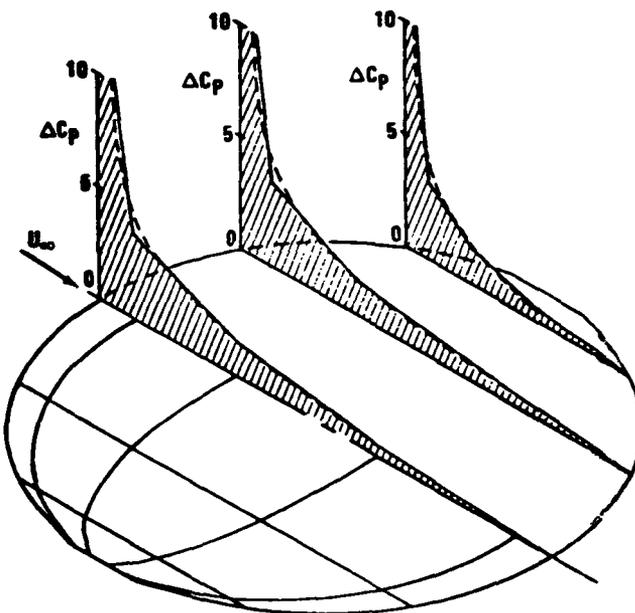
Root Mean Square Downwash Error = 1.02×10^{-1}

FIGURE 28 – VARIOUS PANELINGS OF A CIRCULAR WING

given paneling using a linear chordwise representation. The stability of the solution does not depend on paneling, and the solution converges to the exact results as the number of panels is increased.

6.0 SHELL REPRESENTATION USING THE SPLINE SCHEME

6.1 General Approach

This section presents a scheme which represents the interference effects on wing-body combinations. The basis for this representation is presented in Reference 1 where it is referred to as an interference shell. The shell amounts to a cylindrical surface with singularities distributed over it, much the same as for the wing. The interference shell, however, is not a impermeable surface with flow tangency boundary conditions. The purpose of the shell is to account for the mutual interaction between the body and the wing. The shell boundary condition is that the shell singularities induce a velocity which cancels the velocities on the shell that are induced by the wing. The body contained inside the shell, will however, induce a flow through the shell which is not canceled. The enclosed body then appears to be in an undisturbed free stream flow, therefore its analysis can be treated separately using some appropriate technique (e.g., Ref. 12).

The aim of this shell study was to provide an improvement over the constant pressure panel shell (Ref. 1). In so much as the vortex spline arrangement provided much improvement over the constant pressure panel scheme for the wing, it was felt a similar development for the interference shell would be appropriate. There was, however, an unresolved question concerning the interference shell - namely whether the elementary horseshoe vortex was the appropriate singularity needed to model the body-wing interaction effect. The question arose because bodies in potential flow do not have a wake (i.e., shed vorticity) and because the elementary horseshoe vortex does have a wake. This difference between the flow on a wing and the flow on a body can be attributed to the roundness of the aft end of a body as compared to the sharpness of the trailing edge of a wing (suggesting no Kutta condition on a body). If the Kutta condition is not used, a vortex solution is not unique (Ref. 5, pg. 57). This means that a shell representation using the vortex spline which needs the Kutta condition might not properly model the flow on a body. Because of this possibility, a study was initiated whereby several elementary singularities were developed which could be utilized in a spline technique. These singularities were the elementary horseshoe vortex, the source, and the doublet. Unfortunately, none of the analyses was developed to the point of yielding numerical results. The next section shows the analysis which was performed for the various singularities as well as a detailed description of a scheme using the elementary horseshoe

74

vortex in an influence coefficient approach. The scheme described
is compatible with the scheme already presented for wings.

6.2 Interference Shell Singularities

Figure 29 shows the cylindrical coordinate system used to analyze the interference shell. Since the doublet and elementary horseshoe vortex can be derived from the source (Ref. 5, pp. 28 and 87), the analysis will begin with the source singularity for subsonic flow.

The elementary source potential, Φ_s, for subsonic flow is given as (Ref. 5, pg. 87):

$$\Phi_s(x,r,\theta) = \frac{-1}{4\pi} \frac{1}{\sqrt{(x)^2 + \beta^2 r^2}} \qquad (65)$$

where $\beta^2 = 1 - M^2$. In this expression, the source has been placed at the origin of the coordinate system. If however, the source is located at some other point (x_0, r_0, θ_0), then the potential becomes θ dependent:

$$\Phi_s(x,r,\theta,x_0,r_0,\theta_0) = -\frac{1}{4\pi \sqrt{(x-x_0)^2 + \beta^2(r^2 + r_0^2 - 2rr_0\cos(\theta - \theta_0))}} \qquad (66)$$

The above result can be better understood from Figure 30.

The kernel function corresponding to that used for the planar vortex panels can be derived by differentiating (66) with respect to the local surface normal coordinate (i.e., $\partial\Phi_s/\partial r|r=r_0$ is the downwash on a cylinder of revolution). In order to obtain the influence coefficient, A_{ij} this velocity kernel must be multiplied by the proper strength variation chordwise and circumferentially (the latter variation corresponding to the spanwise variation for planar panels). After multiplication, the function must be integrated over the domain of the singularity.

The interference shell can be paneled in a way entirely analogous to the geometric paneling scheme used for the wing (Figure 31). First the cylinder can be divided streamwise by parallel rays on the surface. Then the cylinder can be further divided by parallel planes normal to the axis of the cylinder. These cuts define a group of panels which are rectangular in the $x-\theta$ coordinates. Spline functions for the various singularities can be defined using these panels.

Since the different singularities require different degrees of continuity, the analysis from this point on will be limited to the elementary horseshoe vortex using the continuity conditions
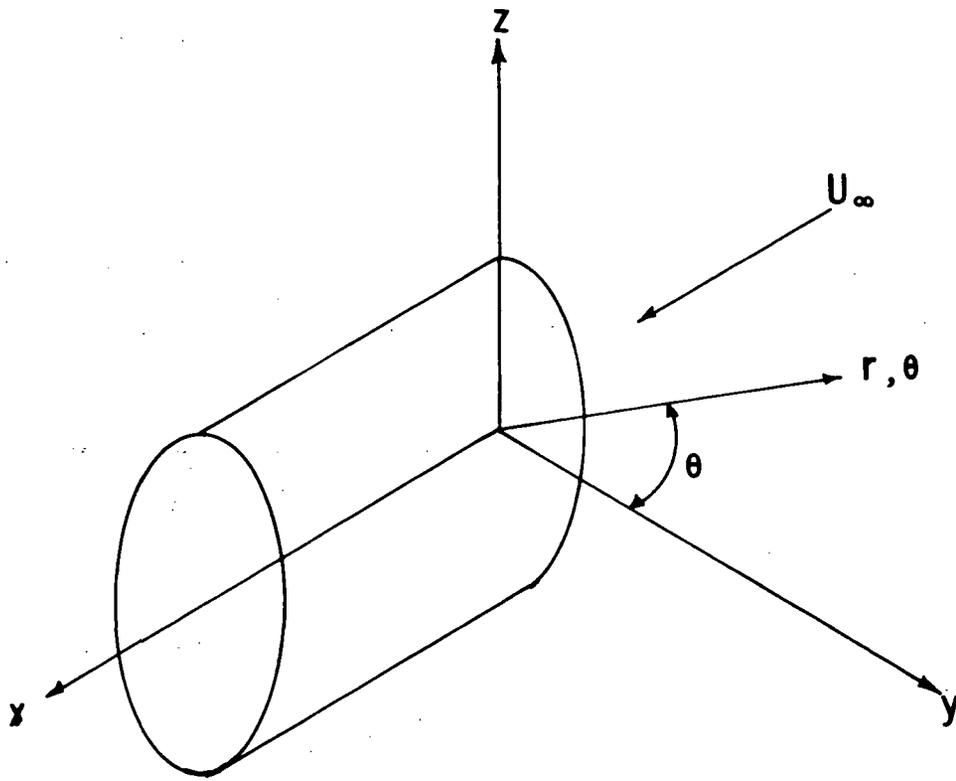
FIGURE 29 – GEOMETRY OF INTERFERENCE SHELL

The figure contains the following labels and equation:

Location of Control Point

$$|\vec{r} - \vec{r}_o| = \sqrt{(r^2 + r_o^2 - 2 r r_o \cos(\theta - \theta_o))}$$

Location of Singularity
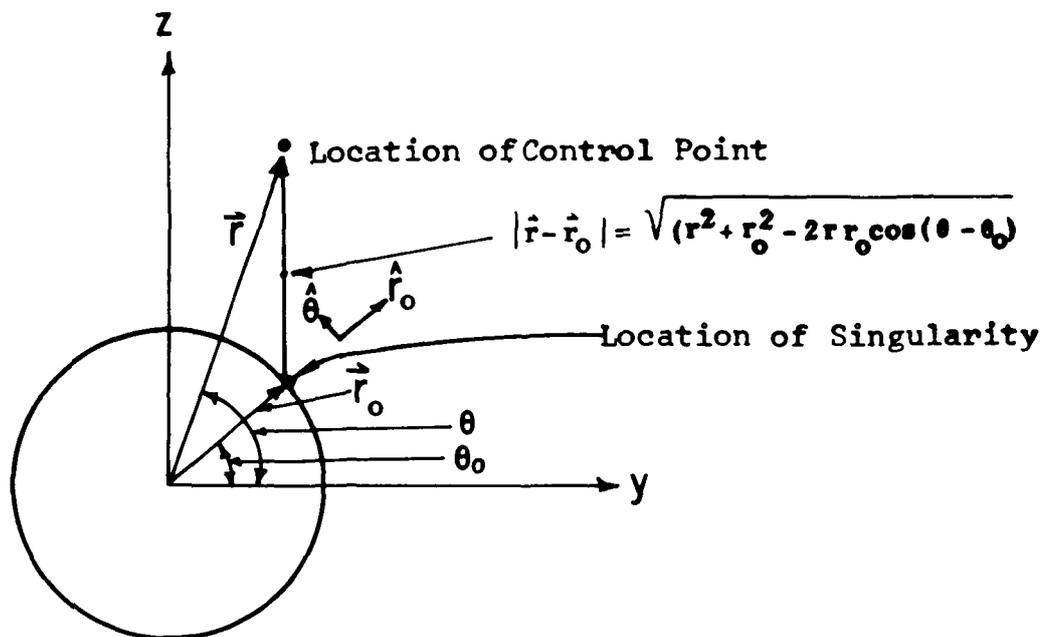
FIGURE 30 - AXIS SYSTEM AND DEFINITION OF VARIABLES
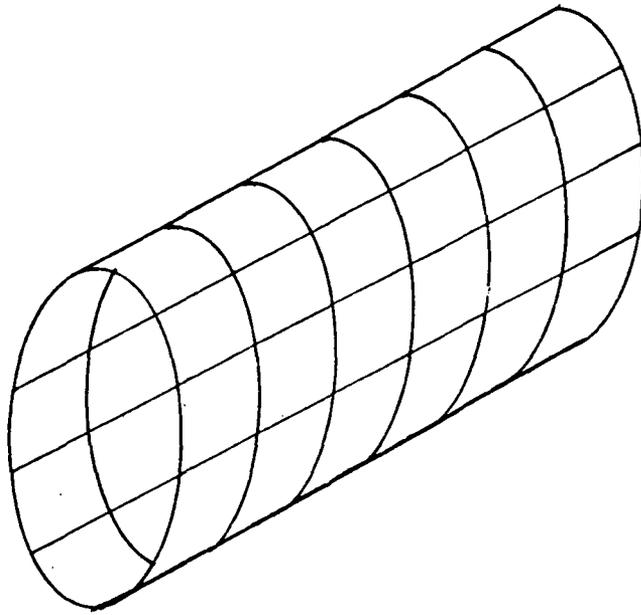
FIGURE 31 - PANELING OF AN INTERFERENCE SHELL
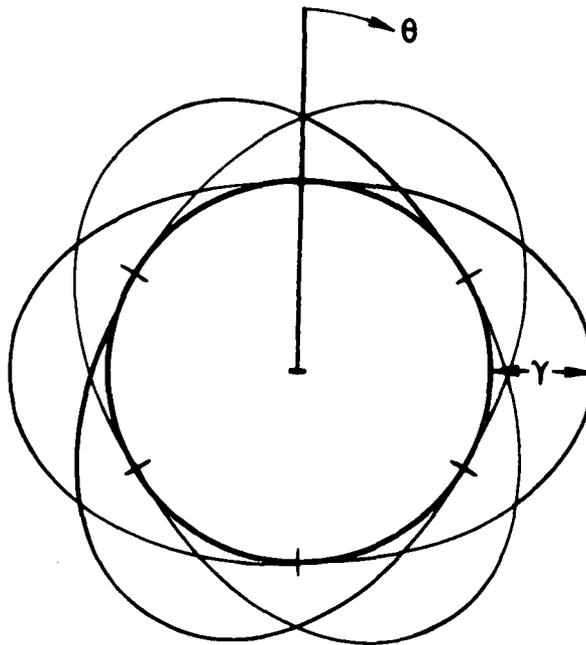
FIGURE 32 - THREE PANEL SPLINE FUNCTIONS ON INTERFERENCE SHELL

79

already defined for planar panels. The analysis will be further restricted to circular cylinders having equal arc length panels.

The first step in the shell analysis is the derivation of the elementary horseshoe vortex on a circular cylinder. This singularity is obtained by integrating the doublet potential function (Ref. 5, pg. 87) from some initial point Xo to ∞ (downstream). This integration corresponds to a line of doublets from the point Xo to ∞ . The potential of the doublet with its axis in the $\vec{r}_0$ direction (Figure 30) is derived by differentiating the source potential (66) with respect to r_0 :

$$\Phi_d(x,r,\theta,x_0,r_0,\theta_0) = \frac{\partial \Phi_s}{\partial r_0} = \frac{\beta^2}{4\pi} \frac{(r_0 - r\cos(\theta-\theta_0))}{\left[(x-x_0)^2 + \beta^2(r^2+r_0^2 - 2rr_0\cos(\theta-\theta_0))\right]^{3/2}} \quad (67)$$

The potential of the elementary horseshoe vortex is then:

$$\Phi_v(x,r,\theta,x_0,r_0,\theta_0) = \int_{x_0}^{\infty} \Phi(x,r,\theta,x_0',r_0,\theta_0)dx_0'$$

$$= \frac{r_0 - r\cos(\theta-\theta_0)}{4\pi(r^2+r_0^2 - 2rr_0\cos(\theta-\theta_0))}\left\{1 + \frac{x-x_0}{\sqrt{(x-x_0)^2 + \beta^2(r^2+r_0^2 - 2rr_0\cos(\theta-\theta_0))}}\right\} \quad (68)$$

For this analysis, a spline arrangement spanning three circumferential panels was used (Figure 32). The circumferential variation can be derived using three quadratics (one on each panel) and a set of constraint requirements. On the first panel (Figure 33), the requirements are that the function must vanish in value and slope at the left edge. On the second panel the requirements are that the function be continuous in value and slope at the left edge. On the third panel the requirements are that the function be continuous in value and slope at the left edge, and vanish in value and slope at the right edge. These eight requirements, coupled with the additional specifications of unit peak amplitude, completely determine the nine coefficients of the three quadratics composing a single spline. The spline distribution of bound vorticity (strength of elementary horseshoe vortex) can then be written as:

$$\gamma_j(x,\theta) = \sum_{\ell=1}^{2}\sum_{m=1}^{3} x_j^\ell \theta_j^m \quad (69)$$

where x_j^ℓ is the same as that defined by Equations (26) and (27), and the θ_j^m for equal arc length panels are:

80
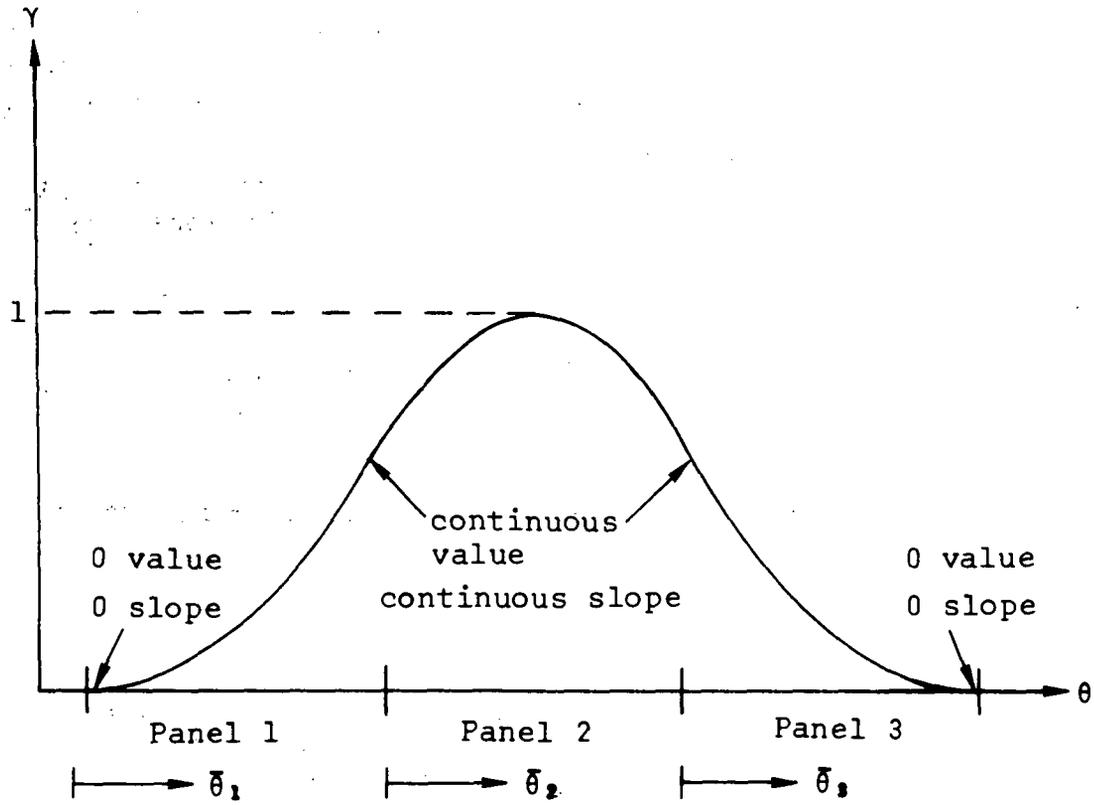
FIGURE 33 - BASIC THREE PANEL SPLINE

$$\theta_j^1 = \frac{2}{3} \bar{\theta}_1^2 \tag{70}$$

$$\theta_j^2 = \frac{2}{3} + \frac{4}{3} \bar{\theta}_2 - \frac{4}{3} \bar{\theta}_2^2 \tag{71}$$

$$\theta_j^3 = \frac{2}{3} - \frac{4}{3} \bar{\theta}_3 + \frac{2}{3} \bar{\theta}_3^2 \tag{72}$$

The $\bar{\theta}$'s are local coordinates for each panel ranging from 0 at the left edge to 1 at the right edge.

The influence coefficient kernel is found by differentiating Equation (68) with respect to r (to find the normal velocity kernel) and evaluating this resulting expression on the surface of the cylinder (r equal r_o).

$$K(x_1, \theta_1, x_o, \theta_o, r_o) = \frac{1}{4\pi} \left\{ \frac{1 - 2\cos\Delta\theta}{2r_o^2(1-\cos\Delta\theta)} \left[1 + \frac{x_1 - x_o}{R}\right] - \beta^2 \frac{(x_1 - x_o)(1-\cos\Delta\theta)}{2R^3} \right\} \tag{73}$$

where $\Delta\theta$ is $\theta_1 - \theta_o$, R is $\sqrt{(x_1 - x_o)^2 + 2\beta^2 r_o^2(1-\cos\Delta\theta)}$, and the subscript "i" denotes that the field point (x, θ, r) is on the cylinder surface.

The influence coefficient is then:

$$A_{ij} = \int_{\theta_L}^{\theta_R} \int_{x_{LE}}^{x_{TE}} \gamma_j(x, \theta) \, K(x_1, \theta_1, x, \theta) dx \, r \, d\theta \tag{74}$$

The integration can be carried out in exactly the same manner as for the planar panels performing the x integration first then using the numerical scheme, previously described, to integrate in the θ direction. This same numerical integration scheme can be used since the cylindrical kernel has the same singular properties as the planar kernel.

82

For supersonic flow, the differences in the cylindrical analysis are the same as outlined for the planar analysis basically the kernel and limits of integration change.

The supersonic source is (Ref. 5, pg. 87):

$$\Phi_s\left(x,r,\theta,x_0,r_0,\theta_0\right) = -\frac{1}{2\pi}\frac{1}{\sqrt{(x-x_0)^2 - \beta^2(r^2+r_0^2 - 2rr_0\cos(\theta-\theta_0))}} \tag{75}$$

The doublet in the $\vec{r}_0$ direction is defined by $\Phi_d = \frac{\partial\Phi_s}{\partial r_0}$:

$$\Phi_d\left(x,r,\theta,x_0,r_0,\theta_0\right) = -\frac{\beta^2\left(r_0 - r\cos(\theta-\theta_0)\right)}{2\pi}\frac{1}{\left[(x-x_0)^2 - \beta^2(r^2+r_0^2 - 2rr_0\cos(\theta-\theta_0)\right]^{3/2}} \tag{76}$$

and the horseshoe vortex is defined by

$$\Phi_v = \int_{x_0}^{x-\sqrt{\beta^2\left(r^2+r_0^2 - 2rr_0\cos(\theta-\theta_0)\right)}} \Phi_d \; dx_0 \tag{77}$$

$$\Phi_v\left(x,r,\theta,x_0,r_0,\theta_0\right) = \frac{1}{2\pi}\frac{r_0 - r\cos(\theta-\theta_0)}{(r^2+r_0^2 - 2rr_0\cos(\theta-\theta_0))}\frac{x-x_0}{\sqrt{(x-x_0)^2 - \beta^2(r^2+r_0^2 - 2rr_0\cos(\theta-\theta_0))}}$$

In the above β^2 is defined as $M^2 - 1$ (β^2 is always positive whether supersonic or subsonic).

The kernel needed for the influence coefficient is derived from (77) by differentiating with respect to r and evaluating the result on the surface of the cylinder (r equal r_0):

$$K\left(x_1,\theta_1,x_0,\theta_0,r_0\right) = -\frac{1}{2\pi}\left[\frac{1}{2r_0^2(1-\cos\Delta\theta)}\frac{(x_1-x_0)}{R} - \beta^2\frac{(x_1-x_0)(1-\cos\Delta\theta)}{2R^3}\right] \tag{78}$$

where $\Delta\theta$ is $\theta_1 - \theta_0$ and R is $\sqrt{(x_1-x_0)^2 - 2\beta^2 r_0^2(1-\cos\Delta\theta)}$

The limits of integration for the supersonic integral are found by determining the intersection of the forward Mach cone, emanating from the control point (x_1, θ_1), with the cylinder.

83

The equation of the Mach cone evaluated on the surface of the cylinder is:

$$\left(x - x_1\right)^2 = 2\beta^2 r^2 \left[1 - \cos\left(\theta_1 - \theta\right)\right] \tag{79}$$

For the simple panels used in the analysis, the intersections are found by replacing x with x_{LE} (x of the leading edge) and x_{TE} (x of the trailing edge). Equation (79) then gives the θ values of the intersections which can be used in the integration limit scheme previously described to establish the region (0, I, or II) and set the limits for the θ integration.

Once the influence coefficients are computed, the boundary conditions are satisfied and remaining analysis is performed using the same logic as was used for the planar development. The boundary conditions of course are different for the interference sell as mentioned before and are more fully covered in Reference 1. However, this difference does not affect the mechanics of obtaining a solution, it only changes the layout of the overall influence coefficient matrix in that the body contained within the shell is assumed to have no influence on the shell.

The above analysis could be repeated using doublets, but since the equivalent doublet strength is the integral of the bound vortex strength in the x direction (Ref. 5, pg. 135), such a formulation would require quadratic distributions in both X and Y. This arrangement could be made using the relations given by Equations (70) through (72) for both the X and θ variations. An influence coefficient scheme could then be formulated which would not shed vorticity. This scheme could then be compared with the vortex scheme to determine the merits of each for body representation. The scope of the present development did not include such a comparison.

7.0 SECOND ORDER SOLUTIONS USING THE VORTEX SPLINE

In the introduction it was pointed out that one of the purposes for developing a new aerodynamic technique was to have a scheme which would calculate those lateral-directional stability derivatives which cannot be handled by the current formulations which treat arbitrary wing-body combinations. The previous sections have shown the development of a scheme which was felt would provide the necessary improvements to meet the lateral-directional requirements. The course of development was to be an initial treatment of planar wings (Ref. 13), then a treatment of bodies in the presence of wings (the interference shell), and finally the treatment of these wings and bodies and their combinations in interaction flow. The initial interaction flow studied was for angle of attack-angle of sideslip.

The basis for the second-order flow analysis is given in Reference 4. In essence, the development assumes that the exact nonlinear, potential flow equation can be expanded in terms of small geometric parameters which define the problem (e.g., angle of attack, angle of sideslip, wing thickness, etc.). When this expansion is carried out, an ordered set of linear equations is obtained. Each of these equations has its own boundary conditions which are determined by a similar expansion of the exact boundary conditions. The higher order equations (those involving powers and products of the small parameters) have non-homogeneous differential equations while the first order equations have the familiar linearized, homogeneous differential equation, e.g.,

$$(1 - M^2) \frac{\partial^2 \phi_2}{\partial x^2} + \frac{\partial^2 \phi_2}{\partial y^2} + \frac{\partial^2 \phi_2}{\partial z^2} = F(x, y, z) \tag{80}$$

$$(1 - M^2) \frac{\partial^2 \phi_1}{\partial x^2} + \frac{\partial^2 \phi_1}{\partial y^2} + \frac{\partial^2 \phi_1}{\partial z^2} = 0 \tag{10}$$

where the subscripts "1" and "2" denote the first and second order terms from the potential flow expansion. The expansion assures that $F(x, y, z)$ is only a function of ϕ_1 and its derivatives.

The forms of these results (Equations (80) and (10)) are standard ones arising from expansions so that the technique used to evaluate results for these equations is general. This point is being made because the expansion in Reference 4 did not properly account for all the terms present and therefore is not valid. Although the result is not correct, the forms of the equations are indicative of the types of numerics needed. The work done in

implementing the technique is therefore valid and would be applicable when the proper expansion is found. Because of this, the technique used to solve the class of problems represented by Equation (80) is presented, but the presentation will be somewhat general in nature. Detailed extension of the scheme to second order wing-body configurations was of course not done.

The solution to Equation (80) consists of two parts - a homogeneous part, ϕ_{2H}, and a particular part, ϕ_{2P}. Since Equation 10 can be added to Equation (80) in any proportion without changing the problem, an assumption is made that a ϕ_{2P} can be constructed which will satisfy the wake boundary conditions. This leaves homogeneous boundary conditions in the wake for the homogeneous solution ϕ_{2H}. This means that the same homogeneous formulation, (i.e., vortex spline) can be used for both first and second order homogeneous solutions. The particular solution, ϕ_{2P}, provides a basic velocity kernel in exactly the same way the horseshoe vortex (homogeneous solution) provided the velocity kernel for the wing and the interference shell (Equation (68)). Following the procedure outlined for the shell, this potential function for ϕ_{2P} is differentiated with respect to the surface normal at the control point. The resulting differentiated quantity is the normal velocity kernel, analogous to those associated with the first order problems for wings and interference shells (Equations (12) and (73), respectively).

Unlike the first order problem the particular solution does not depend on matching the boundary conditions. Rather, the strengths of the distributions and the distributions themselves are known directly and no solving is involved. This is because $F(x,y,z)$ is only a function of the first order problem, whose strength is determined initially in the solution to that problem. Specifically then, the velocity kernel determined from ϕ_{2P} is used to compute an additional influence on the boundary conditions and not used as a means to satisfy them. The downwashes computed from the particular kernel and those obtained from the boundary condition expansion are combined to provide a new set of boundary conditions for the second order homogeneous solution. The homogeneous solution, ϕ_{2H}, is then used to satisfy the combined boundary conditions. The net result is that the combination of ϕ_{2P} and ϕ_{2H} satisfies the boundary conditions for the second order problem which were determined by the initial expansion.

Since the second order homogeneous differential equation is identical to the first order equation, the same basic solution technique can be used (i.e. the vortex spline). The second order homogeneous solution, of course, has different boundary conditions and correspondingly different strengths from that of the first order. Also, depending on which equation is involved, there can be different symmetry requirements for the solution (e.g. angle of

86

attack -angle of sideslip problem assuming zero sideslip is antisymmetric while the first order problem, angle of attack, is symmetric).

Figure 34 shows how a second order problem could be solved using the vortex spline scheme. Basically the central block of logic is the homogeneous boundary condition solver which is the vortex spline scheme (Figure 21). The second order particular solution section of the logic block provides the downwashes which must be combined with the specified boundary condition (from the expansion). These downwashes then represent a new set of boundary conditions for the homogeneous solution (ϕ_{2_H}) which is solved in the exact same manner as the first order problem. The quantities necessary to obtain the pressures are then computed (this is not always just the bound component of vorticity as pointed out in Reference 4) and the stability derivatives are obtained.

The advantage of the vortex spline for solving these second order problems can be seen from a study of the characteristics of the forcing functions $F(x,y,z)$ (Ref. 4). These functions generally involve derivatives of the first order solution. A solution to the first order problem must, therefore, be capable of providing sufficient derivative resolution that the second order problem can be solved accurately. The splines provide this capability as can be seen from Figures 22 through 28.

Geometry
○ Areas
○ Control Point Locations
○ Panel Descriptions

AIC MATRIX Generator
○ A & B

Downwash at Each Control Point Due to Each Function (A= Aerodynamic Influence Coefficient Matrix)*

Least Square Error AIC Matrix Formulator
○ $\tilde{A}^T A$

Least Square Error Downwash Matrix
○ $\tilde{A}^T \{w\}$

Solution - Strengths of Singularities
○ $\{B\} = \left[\tilde{A}^T A\right]^{-1} \tilde{A}^T \{w\}$ (First Order Solution)

$\{w'\} = B\{B\}$

Downwash at Points in Downstream Regions

Downwashes Used For Downstream Regions in Supersonic Flow

Mach Line Paneling Loop

Second Order Particular Solution Bound Calculations

Total First Order Pressures, Loads, and Moments

○ Second Order Particular Solution's Contributions to Pressures, Loads, and Moments

Yes | Additional Regions

No

Error Analysis

○ Average Error & Average Square Error

Downwash Due to Particular Solution ▶ Strengths Computed from First Order Solution i.e.eq.(62)

○ Downwashes at Control Points Due to Particular Solution

(This section is the same as for the first order solution except that the boundary conditions are established by the particular solution and not by the geometry and angle of attack of the model.)

Second Order Homogeneous Solution Circulation Calculations

Yes | Additional Regions

No

Error Analysis

○ Average Error & Average Square Error

○ Computed Quantity

(~) Denotes Weighted Matrix

Total Second Order Loads & Moments

Circulations from Homogeneous & Particular Solutions

Exit

*The influence of the functions on points outside the region of investigation (Matrix B) are also computed. These points are used in the supersonic case to compute the influence of one region (upstream) on another (downstream). This technique allows the solution to be obtained by marching downstream.

FIGURE 34 - CONCEPTUAL FLOWCHART (SECOND ORDER)

8.0 CONCLUDING REMARKS

The experience gained with the vortex spline scheme has indicated the following:

1. The solution is not strongly dependent on paneling arrangement; it works well with uniform or nonuniform panel spacing.

2. The scheme works equally well for both subsonic and supersonic flow.

3. Special Mach line paneling produces better pressure resolution in supersonic flow than geometric paneling. However, in all cases the geometric paneling produced accurate values for lift and moment.

4. The absence of downwash singularities in the wake (except behind planform tips) implies that tails can be paneled independently from wings.

5. Computation times are small, requiring only a few seconds (CDC 6600) for simple planforms and less than 2 minutes for finely paneled planforms.

6. Accurate results can be obtained with sparse paneling.

7. The extension of the scheme to the representation of arbitrary configuration surfaces appears entirely feasible.

8. The numerical stability of the scheme provides flexibility in the application of the method. Such stability is a fundamental requirement for the computation of downwash (camber slope) given pressure (this type of problem solving is termed the design mode).

9. The scheme is self-checking in that the user can judge the accuracy of the numerical representation by simply examining the root mean square error in the downwash. (This rms value seems to be the same order of magnitude as the rms error for the pressure distribution for the cases tested so far.)

Future plans for the scheme should include investigation of an automatic paneling technique wherein the user would only be required to input the vehicle shape and specify an acceptable rms error. The program would then automatically panel the configuration, solve the problem, examine the rms error, and repanel based on the error. This cycle would continue until the specified rms error was achieved. Such a development would lead

to a self-checking scheme that provides results of a predetermined level of numerical accuracy.

9.0 REFERENCES

1. F. A. Woodward, "A Method of Optimizing Camber Surfaces for
    Wing-Body Combinations at Supersonic Speeds, Part 1 - Theory
    and Application", D6-10741, The Boeing Company, prepared
    under NASA contract NAS2-2282, 1965.

2. W. S. Rowe, "Collocation Method for Calculating the
    Aerodynamic Pressure Distributions on a Lifting Surface
    Oscillating in Subsonic Compressible Flow", AAIA Symposium on
    Structural Dynamics and Aeroelasticity, Boston, Massachusetts,
    August, 1965.

3. A. R. Dusto and P. P. Polentz, "The FLEXSTAB Stability and
    Control Computer Program for Flexible Aircraft", Integrated
    Program for Aerospace Vehicle Design (IPAD) Colloquium,
    Langley Research Center, Oct. 2-4, 1972.

4. P. E. Rubbert, "Sideslip of Wing-Body Combinations", D6-
    60160, The Boeing Company, prepared under NASA Contract NAS2-
    5006, May 1972.

5. H. Ashley and M. Landahl, Aerodynamics of Wings and Bodies,
    Addison-Wesley Publishing Company, Inc., Reading,
    Massachusetts, 1965.

6. R. L. Bisplinghoff, H. Ashley, and R. L. Halfman,
    Aeroelasticity, Addison-Wesley, Reading, Massachusetts, 1955.

7. K. W. Mangler, "Improper Integrals in Theoretical
    Aerodynamics", British A. R. C., R & M 2424, 1951.

8. R. Church, "Numerical Quadrature Studies", Sperry Rand
    Research Report, SRRC-RR-64-99, December, 1964.

9. P. Businger and G. H. Golub, "Linear Least Squares Solutions
    by Householder Transformations", Handbook Series Linear
    Algebra, Numerische Mathematik, Vol. 7, pp. 269-276, 1965.

10. E. van Spiegel, "Boundary Value Problems in Lifting Surface
    Theories", Verslagen en Verhandelingen, 22, National
    Luchtvaartlaboratorium, Amsterdam, 1959.

11. R. T. Jones and Doris Cohen, High Speed Wing Theory,
    Princeton University Press, Princeton, New Jersey, 1960.

12. Hsue-Shen Tsien, "Supersonic Flow Over an Inclined Body of
    Revolution", Journal of the Aeronautical Sciences, pp. 480-
    483, 1938.

13. J. E. Mercer, J. A. Weber, and E. P. Lesferd, "Aerodynamic Intluence Coefficient Method Using Singularity Splines", Paper No. 73-123, AIAA 11th Aerospace Sciences Meeting, Washington D. C., Jan. 10-12, 1973.

14. J. H. B. Smith, J. A. Beasley, Diana Short and P. Walkden, "The Calculation of the Warp to Produce a Given Load and the Pressures due to a Given Thickness on Thin Slender Wings in Supersonic Flow", British A. R. C., R & M 3471, 1965.

10.0 APPENDIX

Doublet Characteristic Box Method

This method is an alternate approach to the vortex spline in supersonic flow. The method showed promise but further development was halted when it became evident that a great deal of time would be needed to calculate all the integrals involved for the various building blocks, as well as developing a systematic approach to identify all the "special" Mach lines. There was, however, substantial work done on the fundamentals. This effort is presented below.

The first step in the present work was to identify the "special" Mach lines emanating from planform edge breaks. These lines are used to divide the planform into several different regions. Each of these regions is divided into a network of panels bounded by Mach lines as shown in Figure 35.

The basic building blocks comprising the method were identified. These blocks, along with their controlling parameters, are shown in Figure 36. The building blocks include (see Figures 35 and 36):

I	Regular - Bounded by Mach Lines
II	Two Subsonic Leading Edges
III	One Subsonic Leading Edge
IV	Supersonic Leading Edge
V	Subsonic Trailing Edge
VI	Wake

A planform is represented by a superposition of these building blocks. The singularity distribution on each panel is assumed to be a function of the Mach line coordinates (r, s) Figure 37. The type of singularity distribution that was explored initially was a doublet distribution of the form

$$\Delta\phi = a + br + cr^2 + ds + es^2 + frs + gr^2s + hrs^2 + kr^2s^2 \quad (81)$$

where $\Delta\phi$ is the velocity potential jump across a panel and a, b, ... , k are unknown coefficients. This distribution provides vorticity components that vary linearly and quadratically with r and s as shown in Figures 38 and 39, and insure smooth derivatives of the resulting first order solutions.
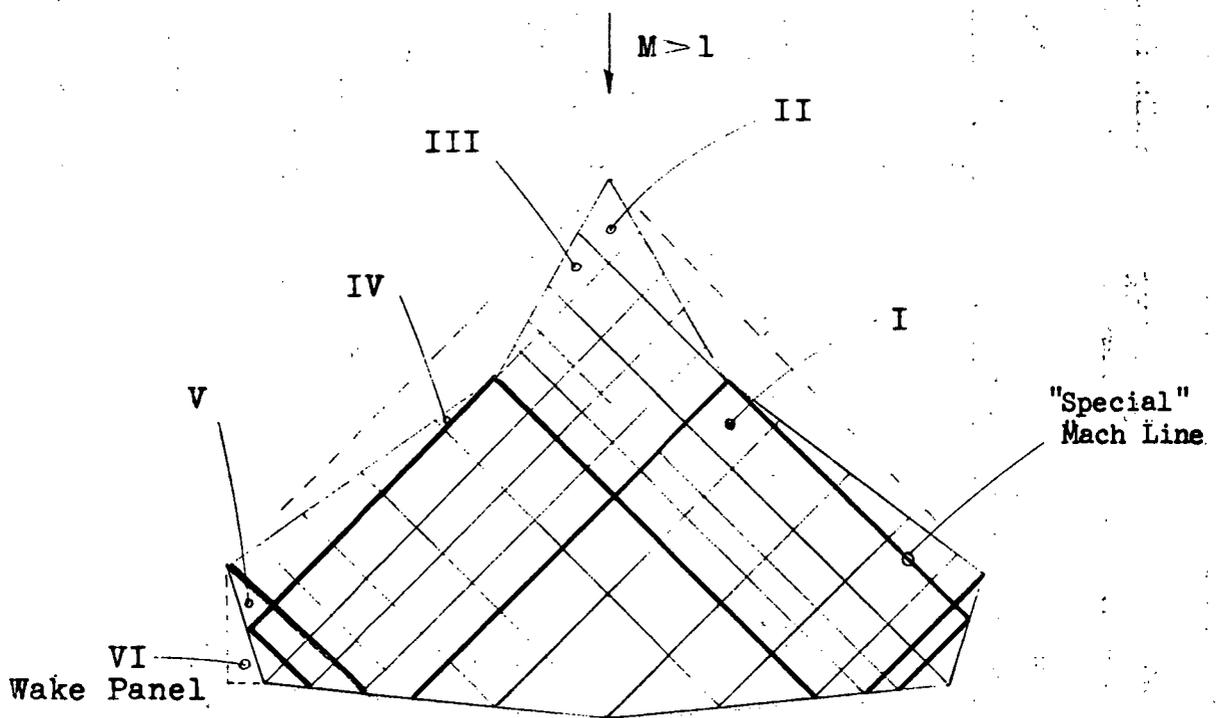
FIGURE 35 - PANELED   PLANFORM

| PANEL	CHARACTER	$\Delta\phi$	$\frac{\partial\Delta\phi}{\partial r}$; $\frac{\partial\Delta\phi}{\partial s}$	FREE PARAMETERS
I – Regular		Given on upstream edges	Given on upstream edges	One downwash Control Point
II–Two.Subsonic Leading Edges		Zero on edges		One downwash Control Point
III–One Subsonic Leading Edge		Zero on free edge, given on upstream edge	May be relaxed	Two downwash Control Points
IV–Supersonic Leading Edge		Zero on edge		Three Control Points along Leading Edge- One Downwash Control Point
V–Subsonic Trailing Edge		Given on upstream edge	Given on upstream edge	Three Downwash Control Points providing the Kutta condition
VI–Wake		Given on upstream edges plus $\Delta C_p = 0$ on entire panel		No Free Parameters

FIGURE 36 - BUILDING BLOCKS

$$s = \frac{M}{2\beta}(x + \beta y)$$

$$r = \frac{M}{2\beta}(x - \beta y)$$

$$\beta = \sqrt{M^2 - 1}$$
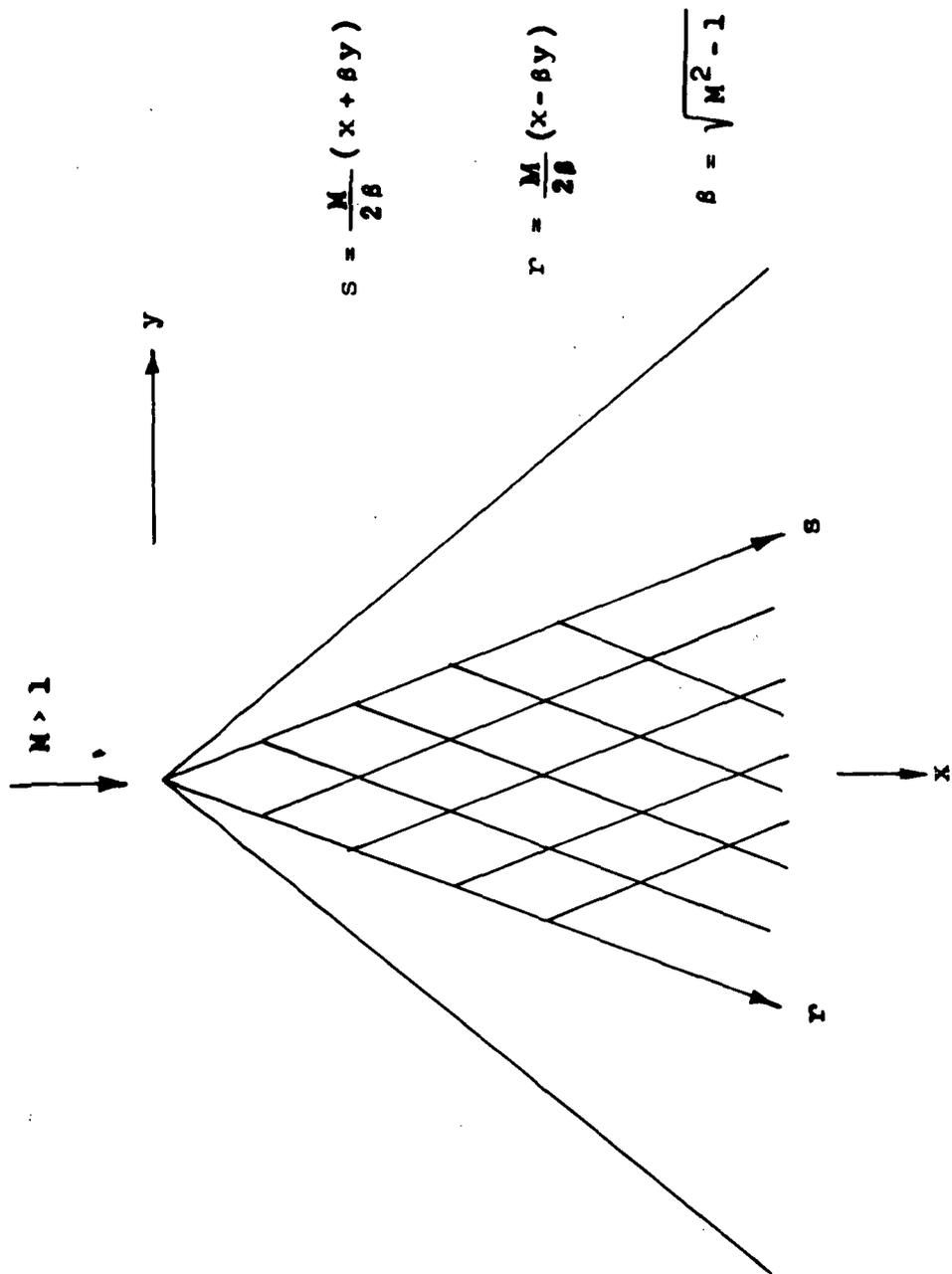
FIGURE 37 - CHARACTERISTIC COORDINATES
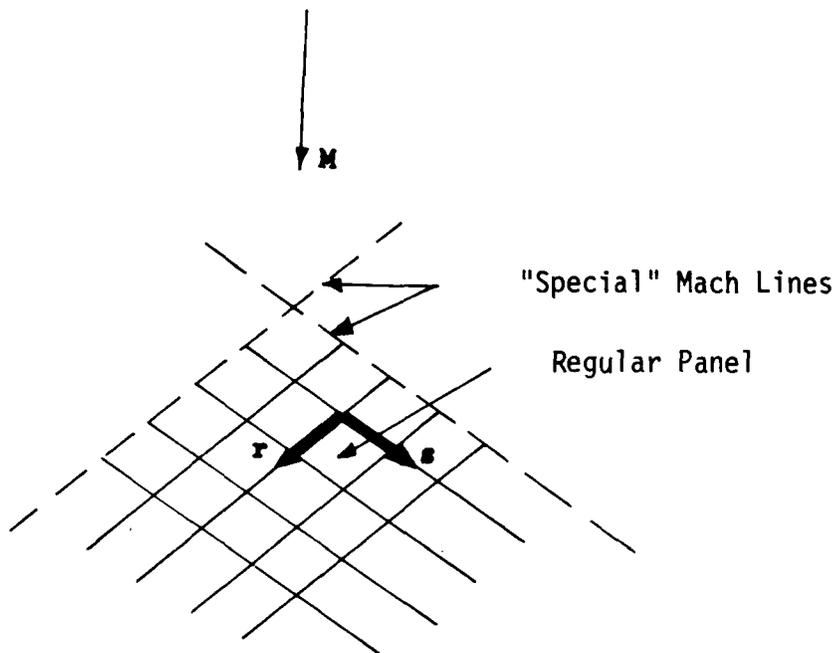
FIGURE 38 - INTERIOR REGION PANELING

Y_r vorticity component parallel to r

Y_s vorticity component parallel to s

$$Y_s = \frac{\partial \Delta \phi}{\partial r}$$

Y_s varies linearly with r

Y_s varies quadratically with s

Y_r varies linearly with s

Y_r varies quadratically with r
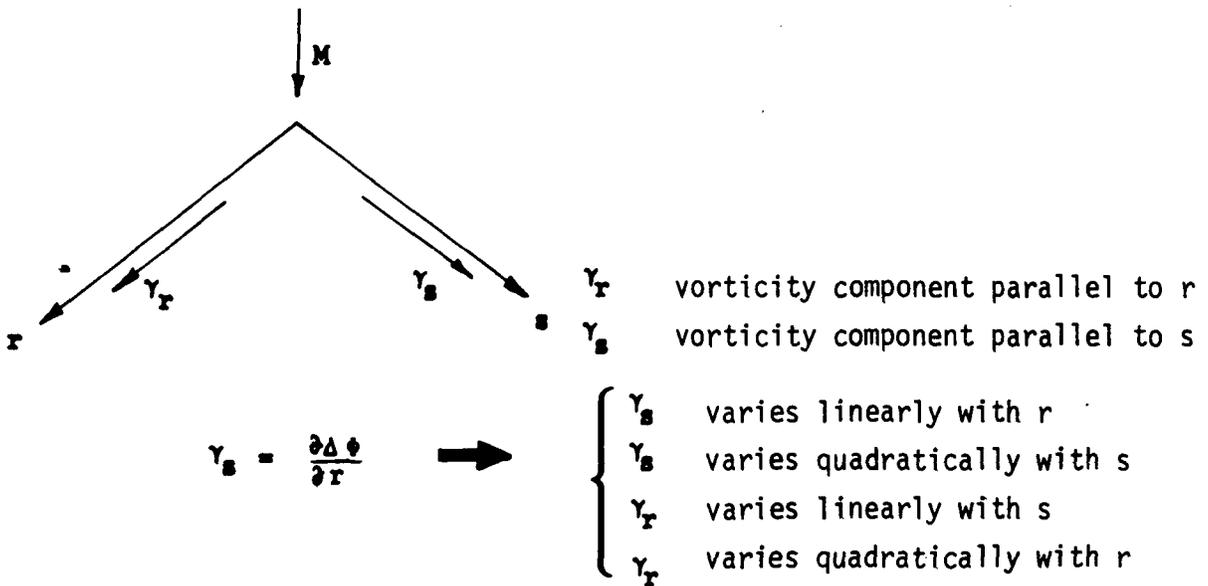
FIGURE 39 - BASIC VORTICITY DISTRIBUTION

The unknown coefficients are found in the following ways: the solution starts with a leading edge panel (II or IV Figure 36) for which $\Delta\phi$ is known (0 at leading edge); the solution then proceeds downstream by matching at common edges. These matching conditions consist of requiring $\Delta\phi$, γ_r, and γ_s (Figure 39) to be continuous across the panel edges. This leaves one free parameter remaining for each panel which is determined by the downwash boundary conditions. The basic method of analysis is shown in Figure 40 for the "Regular" panel. The procedure consists of matching $\Delta\phi$ and the two derivatives, $\partial\Delta\phi/\partial r$ and $\partial\Delta\phi/\partial s$, along the two upstream edges. This leaves only the parameter k as unknown. k is then determined by satisfying the downwash boundary condition at a control point placed on the panel.

Along the network boundaries (either "special" Mach lines or planform edges), some of the matching conditions (i.e., $\Delta\phi$, $\partial\Delta\phi/\partial r$ and $\partial\Delta\phi/\partial s$) are relaxed. They are replaced by additional downwash boundary conditions to provide the freedom needed to account for loading discontinuities, Kutta conditions or other constraints. Although the above procedure provides a determinate set of equations, a minimum error technique might also be incorporated to enable multiple boundary points on the panels.

The influence coefficients relate potential jump, $\Delta\phi$, to the downwash, α, through the planar relationship (the basic doublet representation - Ref. 14).

$$\alpha = -\frac{M}{2\pi U_\infty} \frac{\partial^2}{\partial r \partial s} \iint \frac{\Delta\phi\,(r_1,s_1)dr_1 ds_1}{(r-r_1)^{1/2}(s-s_1)^{1/2}} \qquad (82)$$

Here M is the Mach number and U_∞ is the free stream velocity.

Thus, the unknown coefficients are determined by combinations of:

- Downwash (camber)

- Matching - $\Delta\phi$, $\dfrac{\partial\Delta\phi}{\partial r}$, $\dfrac{\partial\Delta\phi}{\partial s}$, ΔC_p

- Minimum Error

An investigation of the various building blocks and the matching conditions provides the results shown in Figure 36. This figure illustrates the matching conditions applied and the number of resulting free parameters, any of which might be relaxed. Note that a wake panel is completely specified (no free parameters) by the upstream conditions.

Δφ and $\frac{\partial \Delta\phi}{\partial s}$

continuous

Δφ and $\frac{\partial \Delta\phi}{\partial r}$ continuous
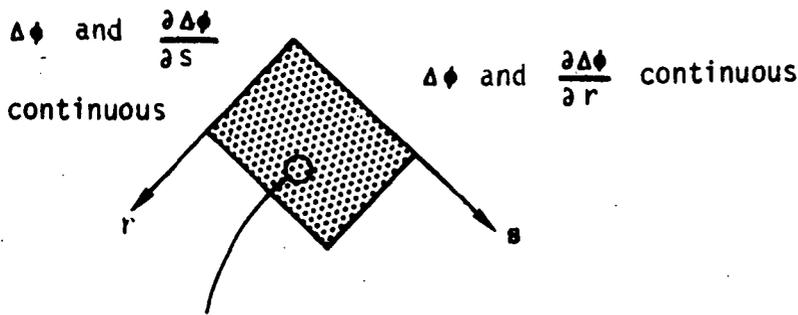
$$\Delta\phi = a + br + cr^2 + ds + es^2 + frs + gr^2s + hrs^2 + kr^2s^2$$

$$\gamma_s = \frac{\partial \Delta\phi}{\partial r} = b + 2cr + fs + 2grs + hs^2 + 2krs^2$$

$$\gamma_r = \frac{\partial \Delta\phi}{\partial s} = d + 2es + fr + gr^2 + 2hrs + 2kr^2s$$

1) At r = 0, Δφ given,

   $a + ds + es^2$ matches the upstream quadratic function

   ∴ a,d,e determined

2) At s = 0, Δφ given ∴ b and c determined as in 1)

3) At r = 0, $\frac{\partial \Delta\phi}{\partial r}$ given, $b + fs + hs^2$ ∴ f,h determined as in 1)

4) At s = 0, $\frac{\partial \Delta\phi}{\partial s}$ given, $d + fr + gr^2$ ∴ g determined as in 1)

5) k unknowns determined from the downwash constraint

   $\alpha \simeq \iint \Delta\phi \, K \, (r, r_1, s, s_1) \, dr_1 \, ds_1$

   where $K \, (r, r_1, s, s_1)$ is the kernel from equation 82.

FIGURE 40 - "REGULAR" PANEL MATCHING

With the sideslip problem in view, the following basic steps were used to make up the doublet characteristic box method.

1) The functional form for the potential jump was selected (i.e., Equation (81)).

2) The boundary conditions are used to determine the parameters of the doublet distribution through combinations of known downwash (camber), matching conditions and methods of minimum error.

3) a) Pressure (and ensuing load) can be found directly as the spatial derivative (in the free stream direction) of the potential jump.

   b) Second order sideslip calculations are made possible by the representations of the velocity potential through the improved spatial derivatives of the first order potential function.

The complexity of the doublet characteristic box method hinges on the downwash-potential jump relationship which must be integrated analytically, numerically, or a combination of the two. Accordingly, the basic downwash-potential jump relationship might be cast into a more suitable form than presented by Equation (82) - such a form might carry the double differentiation under the integral sign, for example.

An investigation of the various building blocks and the matching conditions provides the results shown in Figure 36.

"The aeronautical and space activities of the United States shall be conducted so as to contribute . . . to the expansion of human knowledge of phenomena in the atmosphere and space. The Administration shall provide for the widest practicable and appropriate dissemination of information concerning its activities and the results thereof."
—NATIONAL AERONAUTICS AND SPACE ACT OF 1958

NASA SCIENTIFIC AND TECHNICAL PUBLICATIONS

TECHNICAL REPORTS: Scientific and technical information considered important, complete, and a lasting contribution to existing knowledge.

TECHNICAL NOTES: Information less broad in scope but nevertheless of importance as a contribution to existing knowledge.

TECHNICAL MEMORANDUMS: Information receiving limited distribution because of preliminary data, security classification, or other reasons. Also includes conference proceedings with either limited or unlimited distribution.

CONTRACTOR REPORTS: Scientific and technical information generated under a NASA contract or grant and considered an important contribution to existing knowledge.

TECHNICAL TRANSLATIONS: Information published in a foreign language considered to merit NASA distribution in English.

SPECIAL PUBLICATIONS: Information derived from or of value to NASA activities. Publications include final reports of major projects, monographs, data compilations, handbooks, sourcebooks, and special bibliographies.

TECHNOLOGY UTILIZATION PUBLICATIONS: Information on technology used by NASA that may be of particular interest in commercial and other non-aerospace applications. Publications include Tech Briefs, Technology Utilization Reports and Technology Surveys.

Details on the availability of these publications may be obtained from:

SCIENTIFIC AND TECHNICAL INFORMATION OFFICE

NATIONAL AERONAUTICS AND SPACE ADMINISTRATION
Washington, D.C. 20546